Investigation of Windowless Gas Target Systems for Particle Accelerators

by

William B. Gerber

B.S. Mechanical Engineering, University of Texas (1996)

Submitted to the Department of Nuclear Engineering
in Partial Fulfillment of the Requirements for the Degree of

Masters of Science in Nuclear Engineering

at the

MASSACHUSETTS INSTITUTE OF TECHNOLOGY

June 1998

Author .....
Nuclear Engineering Department
May 10, 1998

Certified by .....
Richard C. Lanza
Senior Research Scientist
Thesis Supervisor

Certified by .....
Lawrence M. Lidsky
Professor of Nuclear Engineering
Thesis Supervisor

Accepted by .....
Lawrence M. Lidsky
Chairman, Departmental Committee on Graduate Students

Investigation of Windowless Gas Target Systems for Particle Accelerators

by

William Gerber

Submitted to the Department of Nuclear Engineering
On May 8, 1998 in Partial Fulfillment of the
Requirements for the Degree of Master of Science in
Nuclear Engineering

ABSTRACT

The application of intense accelerator based neutron sources has been hampered in the past by the material properties of the target system and the requirements of passing the accelerated beam from the vacuum environment of the accelerator to the target. This investigation examines two different methods which remove the limitations of the window in gas target systems.

The first system was initially developed by Iverson at MIT and relied upon low conductance nozzles and rotating disks which opened and closed the beam line. This system achieved pressures up to 75 mbar in the target chamber with pressures below 10^{-3} mbar in the first pumping chamber. Similar experiments conducted by Guzek, Tapper, and Watterson, at Schonland Research Centre at the University of Witwatersrand, were able to reach three atmospheres of pressure in the target chamber. Re-design efforts were conducted to improve the Iverson design and increase the stability of the rotating disks as well as increase the pressure in the target chamber.

The second system examined utilized a "Plasma Porthole" developed by Hershcovitch of Brookhaven National Laboratory. This system relies upon the high pressure and high viscosity of a stabilized plasma arc to support the large pressure differential between the target chamber and first vacuum chamber. Previous experiments conducted by Hershcovitch had supported pressure differences of over 3.5 atmospheres. A system was assembled to fully test the performance of the plasma porthole and compare it against the mechanical system.

With the utilization of windowless gas target systems, the limitations on beam current, energy focusing, and overall power output have been removed. This greatly increases the performance of many applications such as bomb detection in luggage, nuclear stockpile stewardship, and Accelerator-driven Transmutation of Waste (ATW).

Thesis Supervisor: Richard lanza
Title: Senior Research Scientist, Nuclear Engineering Department
Thesis Supervisor: Lawrence Lidsky
Title: Professor of Nuclear Engineering

Acknowledgements

This project was supported by a grant from the Federal Aviation Administration (FAA Grant 93-G-053) as well as funding from Lawrence Livermore National Laboratory.

This project would not have been possible without the help and support of many people. James Hall and Frank Dietrich from Lawrence Livermore National Laboratory gave support in equipment, advice, and ideas. Jim Fraser of Ferrofluidics and the MIT Central Machine Shop gave assistance in designing and producing several of the mechanical components.

Special thanks go to Ady Hershcovitch from Brookhaven National Laboratory. It was through his generous donation of equipment and expertise that allowed for the investigation of the plasma porthole. Similar thanks go to Erik Iverson whose previous work provided the foundation for the mechanical system and whose advice guided the path for the re-design efforts.

Tremendous thanks go to Doctor Richard Lanza and Professor Lawrence Lidsky for their guidance, inspiration, and leadership.

Table of Contents

TABLE OF CONTENTS **4**

LIST OF FIGURES **5**

LIST OF TABLES **6**

CHAPTER 1. INTRODUCTION **7**

1.1 Neutron Sources *7*
Reactors *7*
Isotopes *8*
Accelerators *10*
1.2. Accelerator Targets *12*
Solid Targets *13*
Liquid target *14*
Gas Targets *14*
1.3. Scope of Study *16*

CHAPTER 2. EXISTING SYSTEM **17**

2.1. Accelerator Specifications *17*
2.2. Previous System Theory *20*
2.3. Summary of Implementation (Iverson) *22*
2.4. Pressure Trials *26*

CHAPTER 3. REDESIGN EFFORTS **28**

3.1. Mechanical Changes to System *28*
3.2. Vacuum Pump Alterations *32*

CHAPTER 4. PLASMA ARC THEORY **34**

4.1 Pressure and Density of Plasma Arc *34*
4.2 Plasma Flow *35*
4.3 Focusing Effect *37*

CHAPTER 5. IMPLEMENTATION OF PLASMA ARC **39**

5.1 Plasma Porthole *39*
5.2 System Installation *42*
5.3 Expected Results *43*

CHAPTER 6. APPLICATIONS **44**

6.1 Intense Fast Sources *44*
6.2 Monoenergetic Sources *45*
6.3. Accelerator-driven Transmutation of Waste (ATW) *48*

CHAPTER 7. CONCLUSIONS AND FUTURE WORK **50**

7.1 Comparison *50*
7.2 Future Work *52*

APPENDIX A. PUMP INFORMATION **53**

APPENDIX B. DIAGRAMS OF MECHANICAL SYSTEM **64**

APPENDIX C. DIAGRAM OF PLASMA WINDOW SYSTEM **70**

List of Figures

Figure 1-1: Neutron energy spread from ^{252}Cf spontaneous fission. 9
Figure 1-2: Neutron yields for different systems 12

Figure 2-1: Energies of neutron from D-D reaction..... 20
Figure 2-2: Initial design of mechanical system. 23
Figure 2-3: Cross section of previouse mechanical system. 25

Figure 3-1: Close up view of rotating disks. 29
Figure 3-2: New disk assembly. 31

Figure 4- 1: Focusing from plasma lens on 5 MeV proton beam 38

Figure 5-1: Cross section of plasma porthole 41
Figure 5-2: Plasma porthole system. 42

Figure 6-1: Proof of principal experiment for imaging low-Z material 45
Figure 6-2: Total nitrogen cross-section versus neutron energy 46
Figure 6-3: Total carbon cross-section versus neutron energy 47
Figure 6-4: Accelerator-driven Transmutation of Wast (ATW) target system 49
Figure 6-5: Enlarged view of window system for ATW 49

List of Tables

Table 1-1: Reactions used to produce monoenergetic neutrons..... 11

Table 2-1: Accelerator system specifications from manual 18
Table 2-2: Mechanical system chamber pressures with disk assembly rotating 26
Table 2-3: Mechanical system chamber pressures without disk assembly rotating..... 27

Table 5-1: Achieved pressure differential for Plasma Porthole 43

Chapter 1. Introduction

Since the first discovery of radiation, mankind has been finding new and innovative ways of making use of this new tool. While people currently accept x-ray machines, CAT scans, and many other applications as routine, devices using neutrons have yet to become common place. Neutron imaging and analysis techniques can be used in a wide range of applications including bomb detection in luggage, hydrogen embrittlement in aircraft components, material analysis on both a small and large scale, and many more. In the past, implementation of neutron based technology has been limited by the characteristics of the neutron sources. In order to better utilize neutron based techniques, neutron sources must first be improved.

1.1 Neutron Sources

The three main types of neutron sources regularly used are the nuclear reactor, radioactive isotopes, and accelerator based systems. Each of these systems differ vastly in their implementation and each has its own advantages and disadvantages.

Reactors

The most widely recognized of all neutron sources is the nuclear reactor. Research reactors have been set up across the nation and the world in many colleges, national laboratories, and some private businesses. As an example, the latest research reactor at an U. S. university was built at the University of Texas at Austin and first went critical in 1992. This reactor can produce 1.1 MWs of thermal heat energy and stands

three stories tall. Like most research reactors, long tubes or beam ports are passed through the majority of the shielding surrounding the core of the reactor to allow sufficient radiation to escape for experiments to be conducted. In conjunction with these beam ports, sealed samples can be lowered directly into the core of many research reactors when higher radiation concentrations are required. In general, reactors using ^{235}U fission have a neutron energy spectrum that ranges from a few keV to over 10 MeV with an average of about 2 MeV [1]. Since some amount of shielding must always be present between a beam port and the reactor core, it is difficult to extract high energy neutrons from the core of the reactors. The neutrons that are extracted are present in a large background of radiation consisting of gammas, betas, and heavy charged ions.

Isotopes

The simplest of all sources are radioactive isotope sources. These sources can be conveniently categorized into either a spontaneous fission or a mixed isotope group. The primary spontaneous fission isotopes include ^{254}Cf, ^{252}Cf, ^{244}Cm, ^{242}Cm, ^{238}Pu, and ^{232}U. Most of these isotopes primarily alpha decay with only a very small percentage of fissions. The exception is ^{254}Cf, which decays almost completely by fission with a half-life of 60 days [1]. While it is highly desirable to have this high fission percentage, the half-life is so short that the source is rendered unusable in a very short amount of time. Due to this, the most commonly used fission source is ^{252}Cf. It has a half-life of 2.65 years for fission but only has one neutron decay for every 32 alpha decays. The neutrons emitted from this source have a wide range of energies that are centered between 0.5 and 1 MeV and peak as high as 8 to 10 MeV (Figure 1-1) [2].

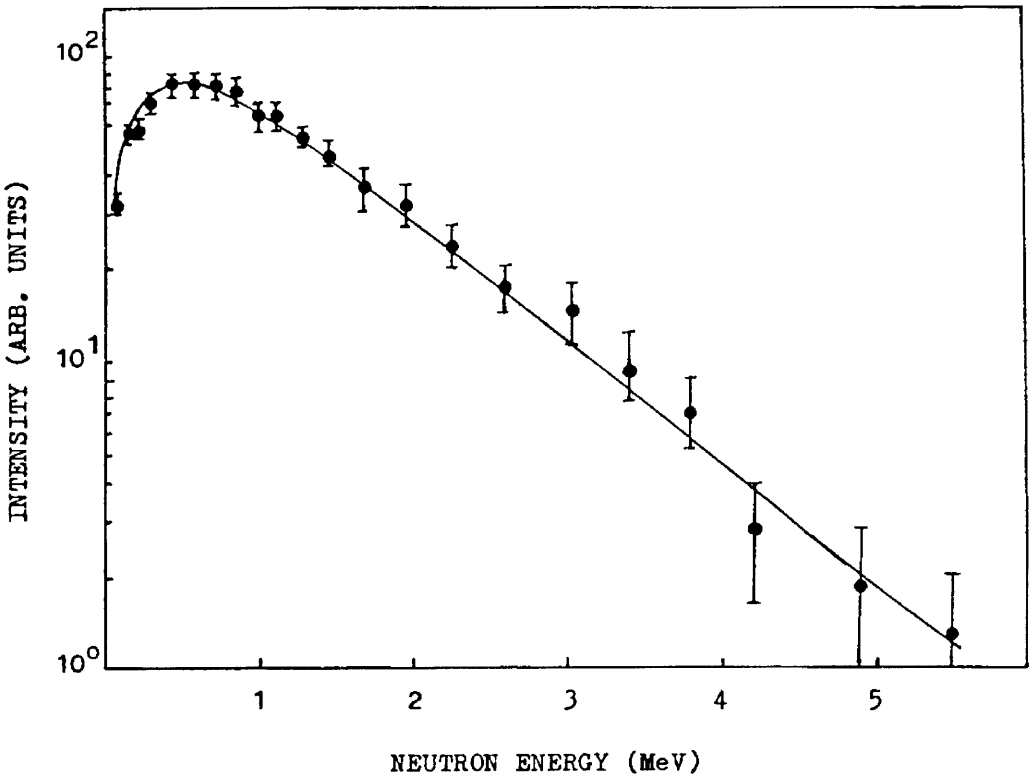

Figure 1-1: Neutron energy spread from ^{252}Cf spontaneous fission [2].

The mixed isotope group contains a variety of different pairs of isotopes combined together where one isotope decays and emits radiation which is then absorbed by the second isotope. This absorbed radiation causes the second isotope to decay and give off one or more neutrons. The type of radiation the first particle gives off can further categorize these types of sources. One of the more common types of these sources uses the (α,n) reaction with beryllium as the most common second isotope. The most common (α,n) source overall uses plutonium 239 as the first isotope and beryllium as the second. A major drawback of these sources is that the alpha particles slow down

greatly in the source before being absorbed by the beryllium. This causes a wide spread in the neutron energy from below 1 MeV to above 10 MeV [2]. A second type of mixed isotope source uses a gamma emitter as the first isotope. These sources have the advantage of being able to emit single energy neutrons. In order for this to happen, the first isotope must emit gammas of only a single energy. The most commonly used isotopes for this are ^{226}Ra, ^{124}Sb, ^{72}GA, ^{140}La, and ^{24}Na. In addition to having only one gamma energy being emitted, the second isotope must not be allowed to end up in an excited state after the release of the neutron. This is accomplished by choosing light target isotopes such as ^{9}Be and ^{2}H [2]. While this system will produce neutrons through the (γ,n) reaction, it will also emit a large background of gamma rays close to 1000 times that of the neutrons [1].

Accelerators

The third and final category of neutron sources is the accelerator-based system. The exact size of an accelerator can vary greatly from the size of a table top to larger than a football field depending on the type of system being used. The main underlying principle of the accelerator system is to use a combination of magnetic and electric fields to accelerate a beam of charged particles into a target. The accelerated particles will then interact with the target nuclei and produce neutrons. While there are many methods to accelerate charged particles, the primary ones are Cockroft-Walton machines, Van de Graff accelerators, linear accelerators, cyclotrons, and synchrotrons. Like the (γ,n) sources, it is desirable to avoid excited states in the target in order to produce monoenergetic neutrons. Some of the common reactions used to produce monoenergetic

neutrons are given in Table 1-1. The most common types of compact accelerator systems rely upon the deuterium on tritium (D-T) or the deuterium on deuterium (D-D) reaction. These systems also have the advantage of having a very small Coulombic barrier which requires minimal particle acceleration between 100 to 300 keV. This is small compared to the Q value of the reactions (17.6 and 3.26 MeV respectively) and allows for easily achieved monoenergetic neutrons. The other reactions listed in Table 1-1 all have larger Coulombic barriers which require the particles to be accelerated to higher energies before entering the target. The choice of accelerated particles and target material also greatly affects the neutron yield (Figure 1-2) [2, 3].

REACTION	Q VALUE (MEV)
$^{3}H(d,n)^{4}He$	17.6
$^{2}H(d,n)^{3}He$	3.27
$^{12}C(d,n)^{13}N$	-0.281
$^{3}H(p,n)^{3}He$	-0.764
$^{7}Li(p,n)^{7}Be$	-1.65
$^{9}Be(p,n)^{9}B$	-1.9
$^{9}Be(d,n)^{10}B$	4.4[a]

[a]The ^{10}B nucleus has excited levels for which Q<0.

Table 1-1: Reactions used to produce monoenergetic neutrons [1,4].

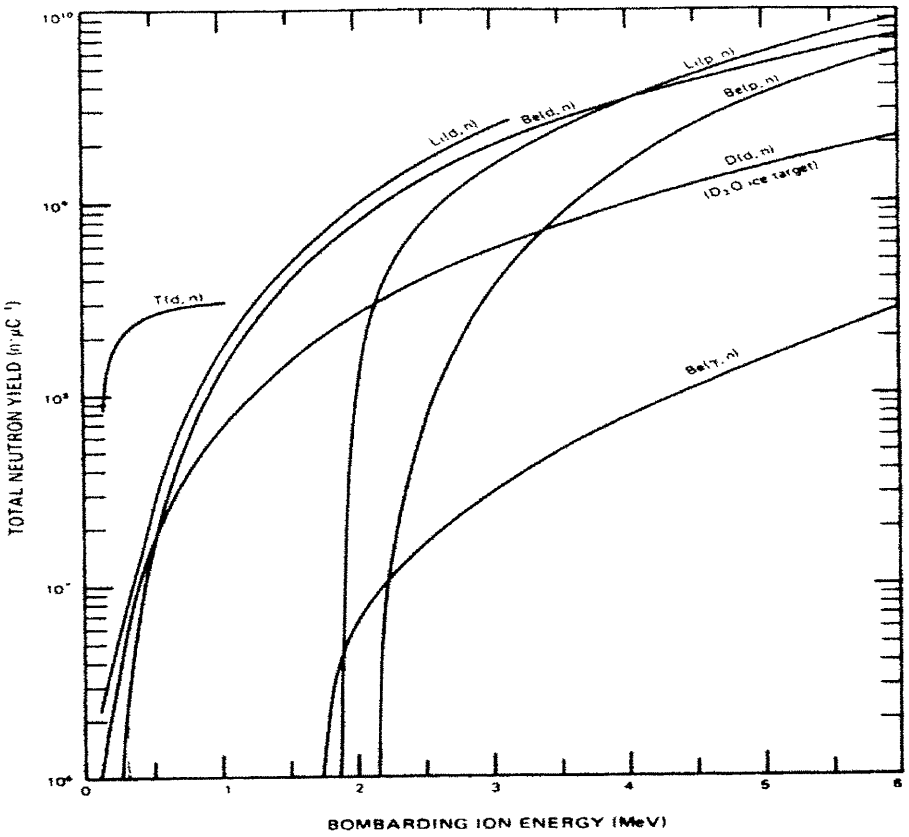

Figure 1-2: Neutron yields for different systems [5].

1.2. Accelerator Targets

Regardless of the method used to accelerate the charged particles, they all rely on the interaction of the particles with a target to produce neutrons. It is during this interaction that some of the major limiting factors for the entire accelerator system are caused. The largest limiting factors are the heat added to the target system as the particles slow down and the spreading of the particle energy during the interaction. If too much heat is added to the target system, it could cause the system to fail, possibly catastrophically. This limitation of dissipated heat limits the amount of charged particles as well as the energy of the particles which enter the target system. The spreading of the particle energy in the

target system causes a subsequent spread in the neutron energy which is often undesirable. Many different designs of target systems have been developed to remove these limitations with varying degrees of success. The primary methods investigated involve either solid targets, liquid targets, or gas targets.

Solid Targets

The simplest type of target system for an accelerator is a solid target. This target is made by joining the desired target atoms to a structural material. For tritium targets this is usually accomplished by infusing tritium into titanium with a ratio of 1.7 tritium atoms to titanium atoms. During the use of this type of target, the neutron yield falls dramatically for several different reasons. First, the tritium involved in the neutron producing reaction is no longer present for future reactions. Also, as the target is heated, the tritium and other metals begin to break chemical bonds and infuse out of the target. Sputtering from the beam also reduces the thickness of the target which decreases the percentage of beam that interacts. Oxidation and chemical deposits on the target change the effective energy of the beam and can hamper heat removal [6]. Due to the large heat deposition, some type of cooling is always needed with solid targets. For a typical target of titanium-tritium layer on a copper or molybdenum backing, a traditional water-cooling system is able to remove heat for beams only up to 1 kW/cm^2. This limits the minimum size of the beam spot as well as reducing the neutron yield to a maximum of 10^{11} n/s [6].

The primary attempt to modify the solid target has been to rotate the target during irradiation. This process spreads the beam spot over a larger portion of the target and lessens many of the problems mentioned above. One such target system is the RTNS-I and then later the RTNS-II located at Lawrence Livermore National Laboratory. By

rotating the target at speeds between 3500 and 5000 rpm, they were able to utilize a 150 mA beam current with approximately 100 kW/cm^2 and extract 3.7x10^{13} n/s [6, 7, 8].

Liquid target

Another type of target system utilizes a liquid target for the accelerator. This flowing target is easier to cool and, due to the constant circulation, it is able to present a continuous fresh target to the beam. One such system was the FMIT and the SUPER-FMIT made by Westinghouse which employed a liquid lithium target. This target streamed a jet of lithium along a slightly curved backwall inside a vacuum chamber. The curvature of the steel backwall applied a compression force on the lithium which aided in preventing the lithium from evaporating. The FMIT was tested with a deuteron beam of 0.1 A and a neutron flux of over 10^{14} n/cm^2. With slight modifications the SUPER-FMIT will be able to use a beam current of 1 A and produce a flux of 10^{16} n/cm^{2}s over a small region [9].

Gas Targets

The third group of targets for accelerators is the gas target system. Since gas has good heat removal properties and can be constantly replenished, the system limitations stem instead from the containment of the gas.

The typical method used to contain the target gas places a thin foil window between the accelerator and the target chamber. These thin windows are designed to pass as much beam through the window as possible while maintaining the structural integrity of the pressurized target chamber. These two different objectives require a compromise in the thickness of the window to be used. In order to maximize the amount of beam that

can pass through, it is desirable to have as thin of a window as possible. However, too thin of a window will not be able to withstand the pressure differential between the vacuum chamber and target chamber.

As the accelerated beam passes through the window, the particles will lose energy, primarily through ionization loss, which causes a spreading in the beam energy and a large heat transfer to the window. This energy loss is more evident in lower energy beams (about 1 MeV or less) since the ionization loss is greater with low energy beams as is shown by the Bethe-Bloch and other relationships. Even with a wide range of different cooling systems, these windows are only able to withstand beam currents in the microAmp range. The initial failure of these windows is a small pinhole leak where the gas diffuses through and into the vacuum chamber. These leaks often reseal after the window returns to room temperature. If the windows are operated too far beyond pinhole leak stage, a permanent leak could be created or total rupture could occur [10, 11, 12, 13].

In a similar method to the rotating solid target, a rotating window system has been designed at Los Alamos. This method extends the life of the total window system but is unable to increase the beam current. As such, it only provides a marginal improvement in the gas target system [14].

Another method to circumvent the limitations of the physical boundary between the high pressure target chamber and the accelerator vacuum chamber has been to remove the physical boundary all together. Since the gas is simple to cool, the problem of heat deposition has been eliminated with the removal of the physical boundary. In this way, higher beam currents and energies can be used and neutron production of 10^{15} to 10^{16} n/s is possible [15]. Many different methods have been tried to accomplish this and most

rely upon the flow characteristics of a jet of gas to support the pressure differential. Trials have been conducted with subsonic, transonic, and hypersonic gas jets along with differentially pumped chambers with flow restricting apertures [15, 16, 17].

1.3. Scope of Study

This study will investigate two separate methods of confining a high pressure gas target chamber from a low pressure accelerator chamber. The first method was initially developed by Iverson [4] and will be reexamined and modified during this investigation. This method utilizes differentially pumped chambers, flow limiting nozzles, and rotating shutters to limit the flow of gas out of the target chamber. The second method investigated utilizes a controlled plasma arc between the target chamber and the vacuum chamber. The high pressure and high viscosity of the plasma will be relied upon to sustain the high pressure differential.

Chapter 2. Existing System

Attempts have already been made by Iverson to create a windowless gas target system. This work relied upon differentially pumped chambers with low conductance tubes in-between and rotating shutters. While this work failed to reach the desired pressures in the target chamber, it did prove the validity of the theory and served as a starting point for this project. The validity of the theory was further proven by experiments that were carried out by Guzek, Tapper, and Watterson which produced target pressures of three atmospheres [18].

2.1. Accelerator Specifications

The starting point for any design of an accelerator based system must begin with the accelerator itself. The accelerator chosen for this experiment was manufactured by AccSys Technology, Inc. and is Model DL-1. It is a radio frequency quadropole (RFQ) linear accelerator which accelerates deuterium particles (Table 2-1). The most critical specifications that directly impact the design of the target system include the maximum duty factor of 2.25%, final deuterium ion energy of 900 keV, and the divergence of the emitted beam.

ACCELERATOR SPECIFICATIONS	
Accelerated particle	d^+
Operating frequency	425 Mhz
Input ion energy	25 keV
Final ion energy	900 keV
Acceptance (normalized)	0.04 πcm-mrad
Current limit	21 mA
Final synchronous phase	-28.0 degrees
Average bore radius	1.60 mm
Maximum vane modulation	2.26
Intervane voltage	45.0 kV
Maximum surface gradient	38 MV/m (1.92xKP)
Cavity RF power (w/o beam)	39.5 kW
Vane length	72.6 cm
Total length	1.016 m
RF drive loop	1 5/8" coaxial
System weight (approximately)	450 lbs
Vacuum pumps (2)	8" cryopump
Design input current	5-15 mA
Input emittance (normalized)	0.02 πcm-mrad
Beam transmission at 10 mA	>90 %
Output energy spread (90%)	<±15 keV
Beam pulse length	5-100 μsec
Cavity fill time	2 μsec
Pulse repetition rate (max)	640 Hz
Total RF power (peak)	48 kW
RF duty factor (maximum)	2.25 %

Table 2-1: Accelerator system specifications from manual [19]

The two main reactions used with a deuteron accelerator are the D-D reaction and the D-T reaction. Since tritium is radioactive, special precautions must be taken at all times during its handling. These extra precautions and added risk are not desirable during these experiments and so the D-D interaction is the only practical choice. Once the system is ready for full implementation, it may be desirable to switch to tritium gas in the target chamber since the D-T reaction is more energetic (17.6 MeV for D-T, 3.27 MeV for D-D). This switch will have a negligible effect on the target system since tritium and deuterium have similar transport characteristics but the safety precautions necessary for handling tritium may preclude this.

The use of the D-D interaction will allow for the selection of specific neutron energies to be emitted. The reaction has a Q of 3.26 MeV and is as follows:

$$^{2}_{1}H + ^{2}_{1}H \rightarrow ^{3}_{2}He + ^{1}_{0}n \qquad (2.1)$$

From the kinetics of the interactions we can solve for the dependence of the exiting neutron energy and get

$$T_b := \left[\frac{\sqrt{m_a \cdot m_b \cdot T_a} \cdot \cos(\theta) + \sqrt{m_a \cdot m_b \cdot T_a \cdot \cos(\theta)^2 + (m_y + m_b) \cdot [m_y \cdot Q + (m_y - m_a) \cdot T_a]}}{m_y + m_b} \right]^2$$

(2.2)

where:

m_a = mass of deuteron — T_a = energy of incoming deuteron

m_y = mass of helium — Q = energy released, 3.26 MeV

m_b = mass of neutron — T_b = energy of outgoing neutron

θ = angle of outgoing neutron with respect to incoming deuteron.

The solution of equation 2.2 over a range of incoming deuteron energies and exiting neutron angles is given in Figure 2-1. This clearly shows that neutron energy can be chosen by fixing the incoming deuteron energy and the exiting angle. Unfortunately, as the deuterons begin to scatter inside the target, ionizing losses will cause their energies to decrease and begin to spread, thus spreading the final neutron energies. This effect is dependent on the thickness of the target and will be greater in thicker targets [2].

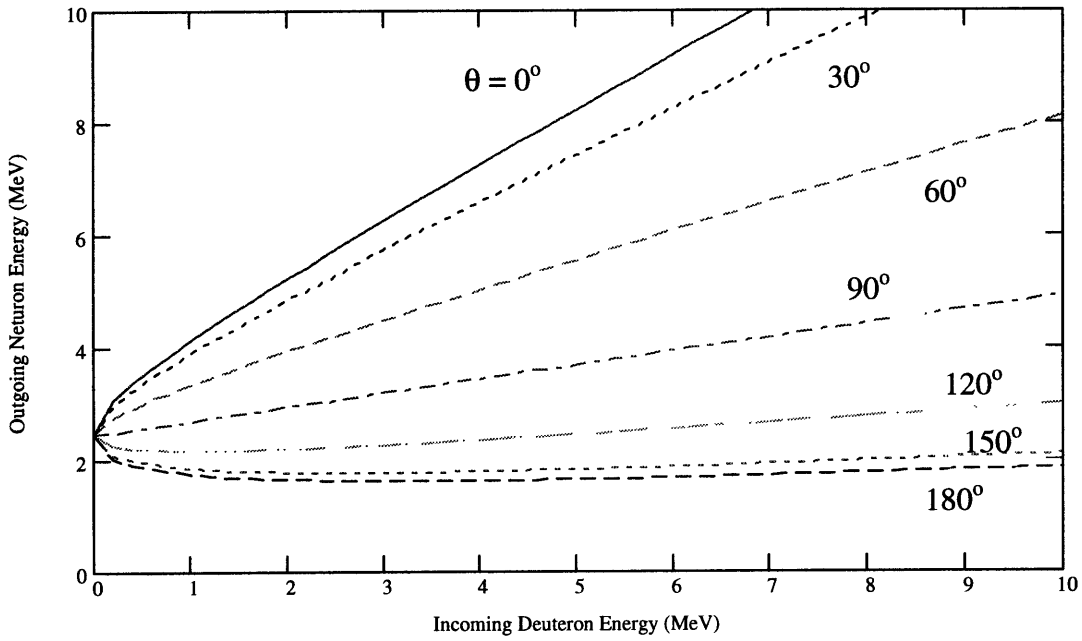

Figure 2-1: Energies of neutron from D-D reaction.

2.2. Previous System Theory

The target system had already undergone two generations of designs before this latest redesign effort began. The initial design attempted to implement a system of pipes in which blocked flow occurred. Blocked flow is the condition where the gas attempts to

flow faster then the speed of sound but is prevented by the buildup of the pressure waves inside the tubes.

The presence of blocked flow inside a tube is dependent on the geometry of the tube, characteristics of the gas, and the pressure differential across the tube. For viscous laminar flow in a tube, the critical exit pressure is given by

$$\frac{p_c}{p} = 2.3 \cdot \frac{d^2}{l} \cdot p \qquad (2.3)$$

where:

p_c = critical exit pressure p = inlet pressure

l = length of tube d = diameter of tube [4].

The flow of air under these blocked conditions is given by

$$q_c = 135 \cdot d \cdot \frac{d^3}{l} \cdot \frac{p^2 - (p_c)^2}{2} \qquad (2.4)$$

where q_c is given in millibar·liters per second [4]. If the flow in the tube is turbulent rather then viscous (Reynolds number greater then 4000) then the critical pressure is given by

$$\frac{p_c}{p} = \frac{4.51 \cdot \left(\frac{d^3 \cdot p^2}{2 \cdot l}\right)^{\frac{4}{7}}}{d \cdot p} \qquad (2.5)$$

and the flow of air is given by

$$q_c = 134 \cdot d \cdot \left[\frac{d^3 \cdot \left[p^2 - (p_c)^2 \right]}{2 \cdot l} \right]^{4.7} \qquad (2.6)\ [4].$$

2.3. Summary of Implementation (Iverson)

After initial testing of several different combinations of pipe lengths and inner diameters, a large four chamber system was created to fully test the design. The system had one target chamber for the pressurized gas and three chambers that would each be evacuated by a pump. The chambers were connected through 5 mm inner diameter pipes which were 10 cm in length (Figure 2-2).

The first chamber to be evacuated was connected to a Roots blower (Pfeiffer WKP 1000). This pump is capable of large flow rates with a lower vacuum limit in the range of 10^{-4} mbar. The Roots blower is incapable of exhausting to atmospheric pressure and is therefore backed up by a large rotary vane pump (Pfeiffer DUO 120A). Together they combine to make the pumping station Pfeiffer WOD-900B. See Appendix A for further pump information. The exhaust of the rotary vane pump is then pumped back into the target chamber with some additional gas added to compensate for leakage.

The second and third pumping chambers are both evacuated by turbomolecular pumps which were chosen for their relatively high flow rates at low achievable pressures. The second pumping chamber is connected to a Pfeiffer TMU 520 and the third chamber is connected to a Pfeiffer TMU 260. They are capable of pumping at 520 liters per second and 260 liters per second respectively (Appendix A) [20]. These pumps are

capable of reaching pressures below 10^{-5} mbar and both are backed by a single rotary vane pump (Trivac D16). This backing pump is then exhausted to the room.

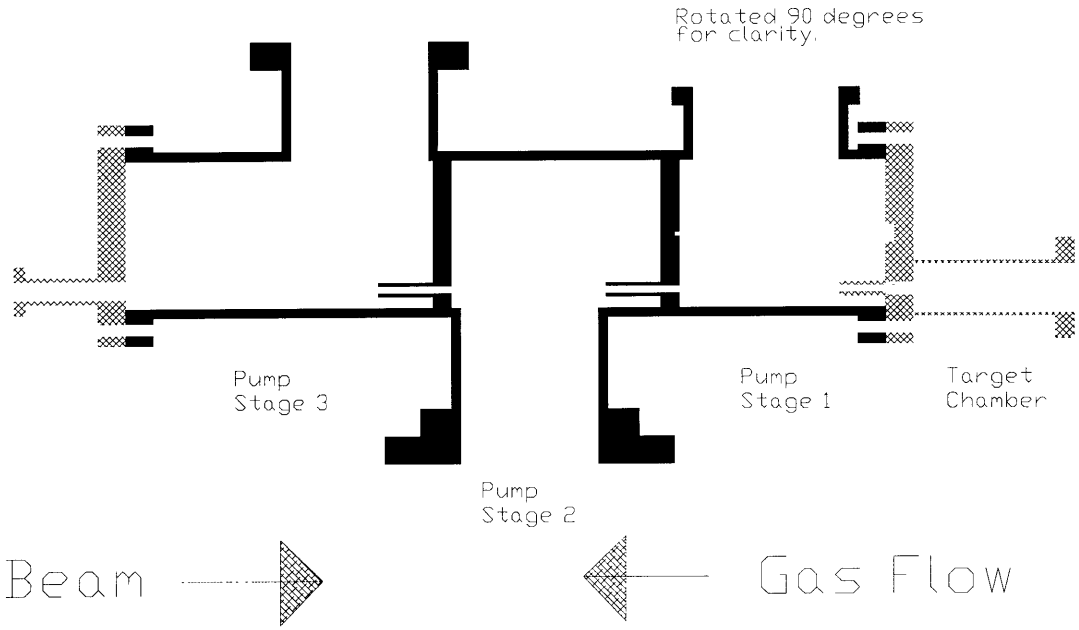

Figure 2-2: Initial design with only pipes.

While initial tests proved promising, it became clear upon implementation that blocked flow was not achieved. The assumption that the pipes could be approximated as long tubes (relative to their diameter) apparently was incorrect. The appropriate assumption now appears to be treating the pipes as exit nozzles from one section to the other [4]. This failure to achieve blocked flow resulted in a vastly increased flow between chambers and greatly reduced the achievable pressure differential throughout the system.

While one option to correct this would have been to elongate the tubes, this would have required that the entire system be lengthened, which was not desirable and any additions to the length would increase the difficulties of the beam optics design. Another option was to have the connections between chambers open only during the pulse of the accelerator. This is possible given that the accelerator has a 2.25% maximum duty cycle. The implementation is made difficult by the high pulse repetition rate of up to 640 Hz. In order to achieve such a high rate of opening and closing of the tubes, it was determined that a system using rotating disks would be the best. As the disks rotate, holes in the disks will line up with the tubes, giving a clear path for the beam to travel during the pulse. The disks would then continue to rotate and thus close off the tubes as the holes no longer line up. Since the beam width is fixed by the duty factor and pulse rate of the accelerator, this establishes the timing for the beam. This timing can then be used to determine the size of the holes in the disks and the overall relationship between the disks and accelerator. This system was implemented with two rotating disks in the first pumping chamber (Figure 2-3). In order to make room for the disks, the tube between the target chamber and first pumping chamber had to be removed.

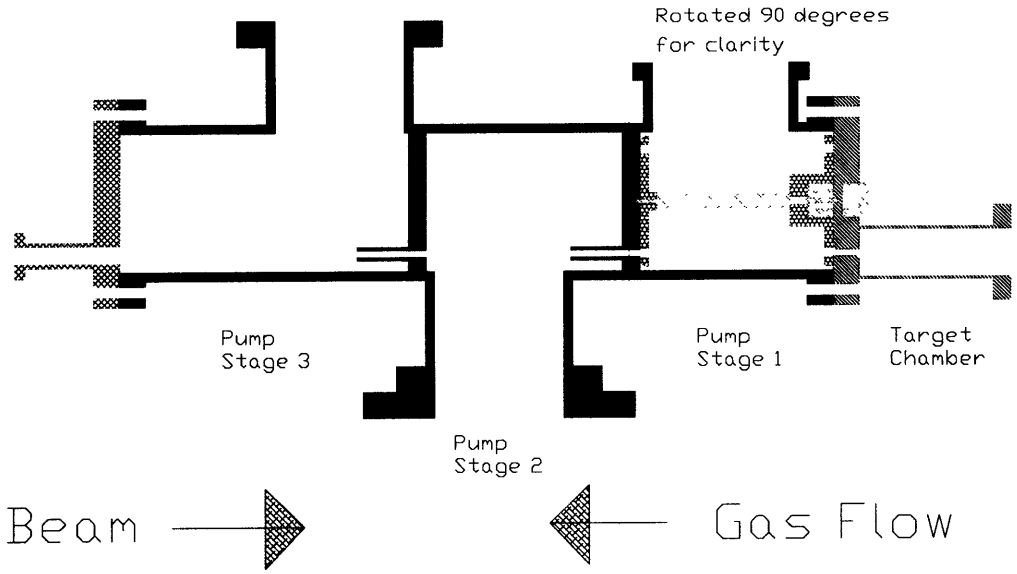

Figure 2-3: Cross section of previous system [4].

The attainable pressure differential in the system is now dependent on the efficiency of the valves. This efficiency was determined by the leak rate of gas around the disks while the disks were in the closed position (holes not lined up). While in the closed position, the gas is able to flow in the space between the disk and the inside wall of the chamber and can escape either around the edges of the disks or through the aperture holes in the disks. To reduce this effect, the disks where machined to fit as tightly as possible into the chamber, thus reducing the gap for the gas to flow between the disks and the walls. Also, the disks were made with only two aperture holes, thus preserving the balance while minimizing the number of paths for the gas to leak.

2.4. Pressure Trials

Once the system was fully assembled and ready for operation, tests were run in order to ascertain the maximum target pressure achievable. These tests were performed first with the beam off and then with the beam on and the pressure results appear in Table 2-2. These experiments demonstrated that the limiting factor was the stability of the rotating disk assembly and not any of the pumps as expected. The pressure in the target chamber could not be increased above 75 mbar without the disk assembly vibrating violently. This instability was mostly due to the pulsing effect created by the jets of gas hitting the disks each time the pathway was opened and closed. As the pressure in the target chamber increased, the force of the jets of air increased, thus limiting the allowable target chamber pressure. Other factors affecting the performance of the spinning disks will be discussed further in Chapter 3.

CHAMBER	PRESSURE IN MBAR	
	Beam off	Beam on
Target	$5.0 \times 10^{+1}$	$4.9 \times 10^{+1}$
1	3.8×10^{-1}	5.1×10^{-1}
2	below 1×10^{-3}	below 1×10^{-3}
3	7.7×10^{-7}	8.6×10^{-7}
Target	$7.3 \times 10^{+1}$	$7.5 \times 10^{+1}$
1	$1.0 \times 10^{+0}$	9.2×10^{-1}
2	below 1×10^{-3}	below 1×10^{-3}
3	1.1×10^{-6}	1.2×10^{-6}

Table 2-2: Chamber pressures with disk assembly rotating [4].

The same pressure measurements were run again but with the disk assembly no longer rotating. This experiment showed what the next limiting factor in the system would be if the disk assembly was sufficiently improved. As the pressure was increased, the second stage pump (TMU 520) was the first to have problems and could not maintain the required flow rate with a target pressure greater than 20 mbar. The pressure results for this experiment appear in Table 2-3.

CHAMBER	PRESSURE IN MBAR	
	Beam off	Beam on
Target	$2.0 \times 10^{+1}$	$2.0 \times 10^{+1}$
1	5.7×10^{-1}	5.3×10^{-1}
2	5.4×10^{-3}	6.7×10^{-3}
3	3.3×10^{-7}	3.1×10^{-7}

Table 2-3: Chamber pressures without disk assembly rotating [4].

During the previous experiment that utilized the rotating disks, the second stage pump (TMU 520) drew less than half the maximum allowable current. This would indicate that in this situation, the target pressure could be operated three to four times higher before the second pump limited the system [4].

Chapter 3. Redesign Efforts

While the final work by Iverson failed to reach the desired pressure range in the target chamber, it did manage to prove the validity of the idea of exit nozzles and spinning disks. The largest improvements in the system will be gained by improving the weakest part of the system, the design of the spinning disks. Other improvements in the overall performance of the system will also be gained through modifying the pumping system.

3.1. Mechanical Changes to System

As stated before, the instability of the disks at pressures above 75 mbar was primarily caused by the pulsing effects of the jets of gas created each time the pathway was opened and closed. While it is impossible to remove these jets, it is possible to improve the structural characteristics of the spinning disk assembly to better resist these effects.

The primary weakness in the spinning disk assembly is the structural support of the shaft at either end. The existing design of the spinning disks has both disks attached to a rotating 9.5 mm diameter shaft. The shaft is decreased in size at both ends to 3.2 mm diameter and is supported by small bearings (Figure 3-1).

A magnetic clutch assembly controls the rotation of the shaft. In this assembly, one side of the magnetic clutch is imbedded in the first spinning disk. On the other side of the target chamber plate, the second half of the magnetic clutch assembly is mounted. In this way, the second half is exposed to atmosphere and can be rotated by a standard electric motor. While this method preserves the integrity of the plate and removes the

need for any feedthroughs, it limited the rotational speed of the assembly to 750 rpm. Since there are only two holes in the disks, this reduces the pulse rate of the accelerator from 640 Hz to 25 Hz [4].

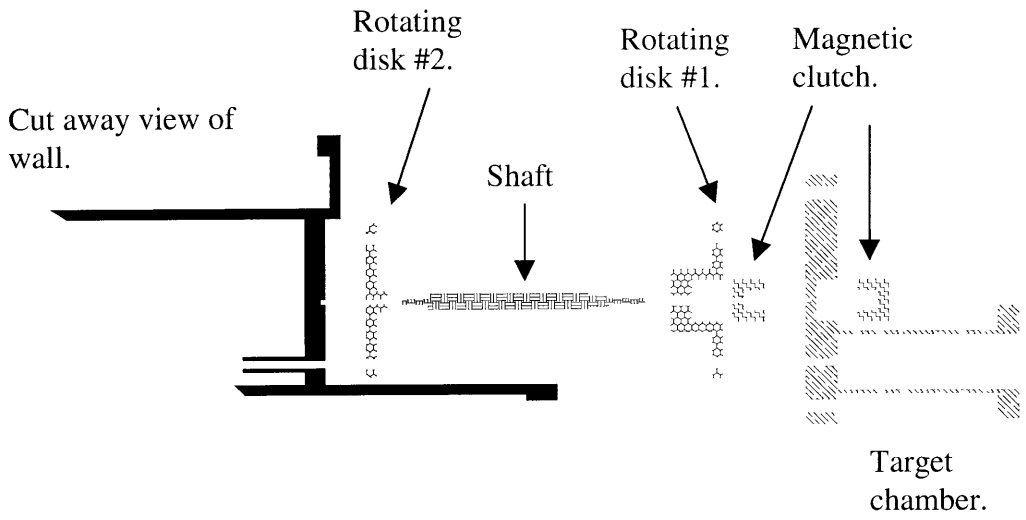

Figure 3-1: Close up view of rotating disks.

Since the magnetic clutch system is unable to rotate the system at sufficient speeds, it was determined that a direct drive system would be better. The simplest implementation of such a system involves replacing the magnetic clutch with a rotary feedthrough. This allows for one solid shaft to pass through the target plate while maintaining the vacuum seal. In order to achieve the maximum pulse rate of 640 Hz with only two holes in the disks, the assembly must be rotated at about 6,000 rpm. This high rotational speed presents a challenge for maintaining the vacuum seal around the rotating

shaft in the feedthrough. This can be accomplished by using rotary seals which employ a magnetic fluid to achieve a seal. A feedthrough capable of such high speeds was procured from Ferrofluidics after some adaptations were performed to allow it to mate with the rest of the system [21].

In order to stop the disk assembly from vibrating, the 9.5 mm diameter shaft and support system were replaced. The shaft diameter was increased to 12.7 mm. This added rigidity should reduce flexing in the shaft and dampen oscillations. With the increase of the shaft and the addition of a feedthrough into the system, it was now possible to pass the shaft through all three pumping chambers and then out into atmosphere. This allows for the expansion of the two spinning disk system to include a third spinning disk in the third pumping chamber. This additional disk will greatly reduce the flow of gas from the second pumping chamber and improve the overall performance of the system (Figure 3-2).

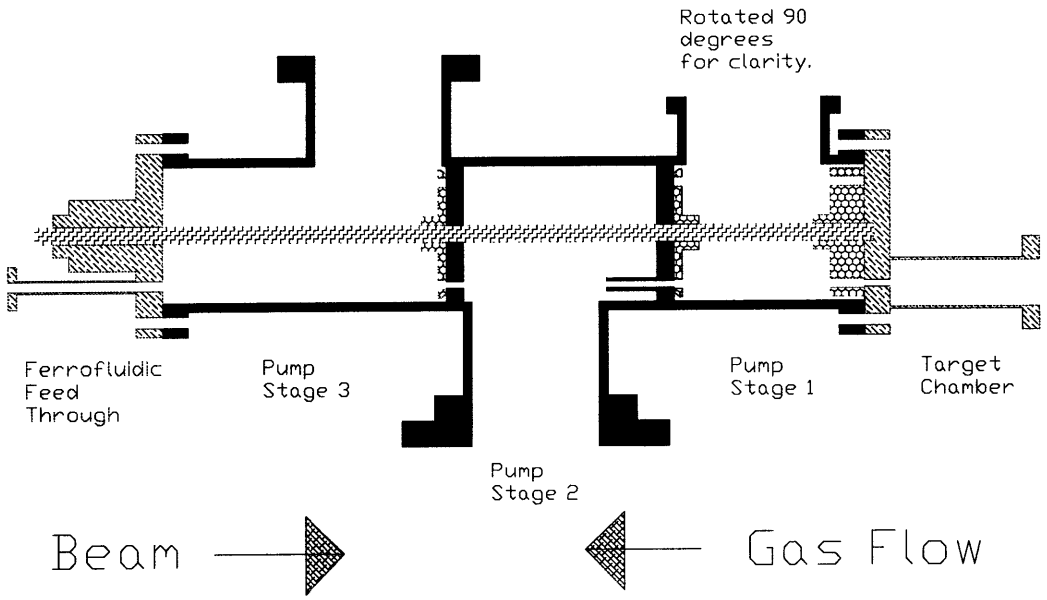

Figure 3-2: New disk assembly.

The two small 3.2 mm bearings that were supporting the original shaft have been completely removed. The shaft is now supported at one end by the feedthrough and at the other end by a 12.7 mm inner diameter bearing. No supports were included in the inside walls of the chamber to avoid possible misalignment that would cause stress on the shaft. Instead, exclusion seals from Ferrofluidics provide a stress free seal that prevents leakage of gas around the shaft from one chamber to the next.

The thickness of the first disk was increased to 25.4 mm in order to limit the leakage of gas around it. This increase creates a longer path that any gas must take as it leaks around the edge of the plate. This longer path restricts the flow and should greatly reduce leakage around the disk. In order to save weight, material is removed from the

side of the disk away from the wall. Unfortunately, the thickness of the second and third disks could not be increased without obstructing the side pipes which connect to vacuum pumps. As such, these two disks are made in a similar manner to the second disk in the original design. See Appendix B for further information on system components.

At the high revolution speed of 6,000 rpm, balancing the disk assembly becomes critical. While the disks have been designed and machined to maintain this balance, further balancing is still needed. Once the entire system has been assembled, it will be brought to an appropriate machine shop, rotated at high speeds, and professionally balanced. This will remove any minor imperfections that would create problems at high rates of revolutions.

3.2. Vacuum Pump Alterations

The initial Roots blower system utilized for the first pumping stage relied upon a rotary vane pump (Pfeiffer DUO 120A) to provide backing pressure for the Roots blower (Appendix A) [20]. This rotary vane pump contains oil in the pumping chamber which was then introduced into the re-circulated deuteron gas. In order to prevent this the vane pump was replaced with the UniDry 050 dry pump from Pfeiffer vacuum (Appendix A) [20]. This pump is specifically designed for high volume flow rates and is ideal as a backing pump for the Roots blower. The combination of the existing Roots blower and the UniDry 050 pump allows for the same high volumetric flow rate as with the rotary vane pump, but with totally dry pumping chambers.

A major design consideration of the windowless gas target system is the re-circulation of all of the gas that leaks out of the target chamber. While this re-circulation

is critical in the first pumping stage, which has the highest flow rates, it is also beneficial in the second and third stages. The current design of the system utilizes a rotary vane pump (Trivac D16A) as a backing pump for the turbomolecular pumps (Pfeiffer TMU 520 and TMU 260, Appendix A) in chambers two and three [20]. This rotary vane pump exhausts the deuterium gas, which is expensive and explosive, into the room. The loss of gas was acceptable at the low flow rates previously achieved, but may prove unacceptable when the target pressure is raised higher. In order to re-circulate the gas, the rotary vane pump will be replaced with a dry pump and connected back into the target chamber. While another dry backing pump could be purchased, the simplest solution is to utilize the same UniDry 050 for the Roots blower and both turbomolecular pumps. This is possible because of the high flow rate capability of the UniDry 050, but the increased load from the turbomolecular pumps will decrease the flow rate through the Roots blower [22]. This decrease will be marginal since the turbomolecular pumps can only pump a fraction of the capacity of the Roots blower.

Chapter 4. Plasma Arc Theory

Another promising method to support a large pressure differential has been investigated by Herschovitch at Brookhaven National Laboratory. This method creates a plasma arc between the high pressure target chamber and the first vacuum chamber. Since the plasma is at very high temperatures, its pressure is equal to that of the target chamber while its density is reduced by the ratio of arc to target temperature. The high viscosity of such a system greatly limits flow through the plasma chamber and serves to confine the gas inside the target chamber. Experiments by Herschovitch have resulted in pressure differentials of close to four atmospheres with minimal pumping from the vacuum chamber. The theory of the plasma porthole and the implementation of it into a pumping system will be discussed in this and following chapters [23, 24, 25, 26].

4.1 Pressure and Density of Plasma Arc

The plasma arc to be used in this experiment will have a temperature ranging from around 15000 K in the center to around 12000 K at the edges [23]. For a general approximation, we can treat the plasma as an ideal gas and use the ideal gas equation

$$P = \rho \cdot R \cdot T \qquad (4.1)$$

with:

P = pressure T = temperature

ρ = density R = ideal gas constant.

Using this equation to compare the density of the plasma arc at 12000 K to the density of the gas in the target chamber at 300 K, it is clear that the plasma is 40 times

less dense while at the same pressure. This low density at high pressures will be key in allowing the plasma to support a large pressure differential while still allowing the accelerated deuteron beam to pass through with minimal interactions.

4.2 Plasma Flow

The pressure differential that the plasma arc will be able to support is determined by the amount of flow of the plasma. This flow is highly dependent on the physical boundaries of the system as well as the physical characteristics of the plasma.

The system is composed of a two millimeter diameter, six centimeter long pipe. As will be shown shortly, the flow of the plasma through the pipe can be approximated as an ideal gas. For low flow through a small thin tube, the flow rate can be given by

$$Q = \frac{\pi \cdot R^4}{8 \cdot \mu} \cdot \left(\frac{dp}{dx} \right) \qquad (4.2)$$

where:

Q = flow rate R = ideal gas constant

μ = viscosity dp/dx = pressure difference in pipe.

It is clear from the above formula that in order to minimize the flow through the pipe while maximizing the pressure differential, it is desirable to increase the viscosity as much as possible [23, 24, 27].

While a complete derivation of the viscosity of the plasma arc would be beyond the scope of this report, a more approximate derivation of the viscosity of gases will be shown.

The type of interactions that are dominant in a gas or plasma system can be estimated by the Knudsen number, Kn, for the system

$$Kn = \frac{\lambda}{L} \qquad (4.3)$$

where:

λ = the mean free path L = a characteristic length for the system.

A Knudsen number of much less than one implies a flow regime dominated by intermolecular collisions. This type of flow is deemed viscous and is common at normal pressures. A Knudsen number much greater than one implies a system where intermolecular collisions are highly infrequent and the molecules act independent of each other. This type flow is termed molecular flow and is present in high vacuum systems. The third type of flow is when the Knudsen number is around one and this is termed transition or slip flow conditions [28].

For this system, L is the diameter of the pipe, 2 mm. The mean free path can be found from the simple relationship

$$\lambda = \frac{1}{n \cdot \sigma} \qquad (4.4)$$

where:

n = molecular density of the gas

σ = cross section of intermolecular collisions.

For this system, n can be found from the ideal gas equation for a gas at 12000 K and a pressure of 2 atm (4.1). A typical value for σ is 10^{-19} m^2 [28]. Hence, the mean free path is $1.6*10^{-5}$ m. This gives a Knudsen number of 0.007, which is much less than one, and implies that the plasma present is dominated by intermolecular collisions. Due to this, the plasma can be approximated as a high temperature ideal gas with little loss of accuracy [29].

Treating the plasma as a high temperature gas simplifies the treatment of the system. Typical fluid mechanics shows that viscosity is directly proportional to the square root of temperature [28, 27].

As the plasma gas is raised in temperature and the intermolecular collisions become less of a factor, this approximation begins to fail. Eventually, the plasma can be treated as fully ionized, at which point the viscosity becomes directly proportional to temperature [30]. It is important to note that this plasma is in the absence of any applied magnetic field.

4.3 Focusing Effect

An added benefit gained from the use of the plasma window is a focusing effect of the deuteron beam. As current flows in the plasma arc it creates a circular magnetic field around the center of the plasma which results in a field in the θ direction. As the positively charged deuteron particles pass through the plasma they interact with the magnetic field and feel a force towards the center of the tube which can be determined by

$$F = q \cdot \vec{v} \times \vec{B} \tag{4.5}$$

where:

q = charge of the deuteron v = velocity

B = induced magnetic field.

This focusing effect on accelerated beams has been investigated as a replacement for other beam optics [31, 32]. These "plasma lenses" are able to focus the beam in the x and y direction simultaneously while other methods, such as permanent magnet quadropoles

(PMQs), can only focus the beam on one axis while increasing the beam on the other. The amount of focusing achieved is highly dependent on the power inside the plasma arc as well as the characteristics of the beam. Figure 4-1 shows the results from an experiment in which a 5 MeV proton beam was focused by a plasma lens of varying voltages [31].

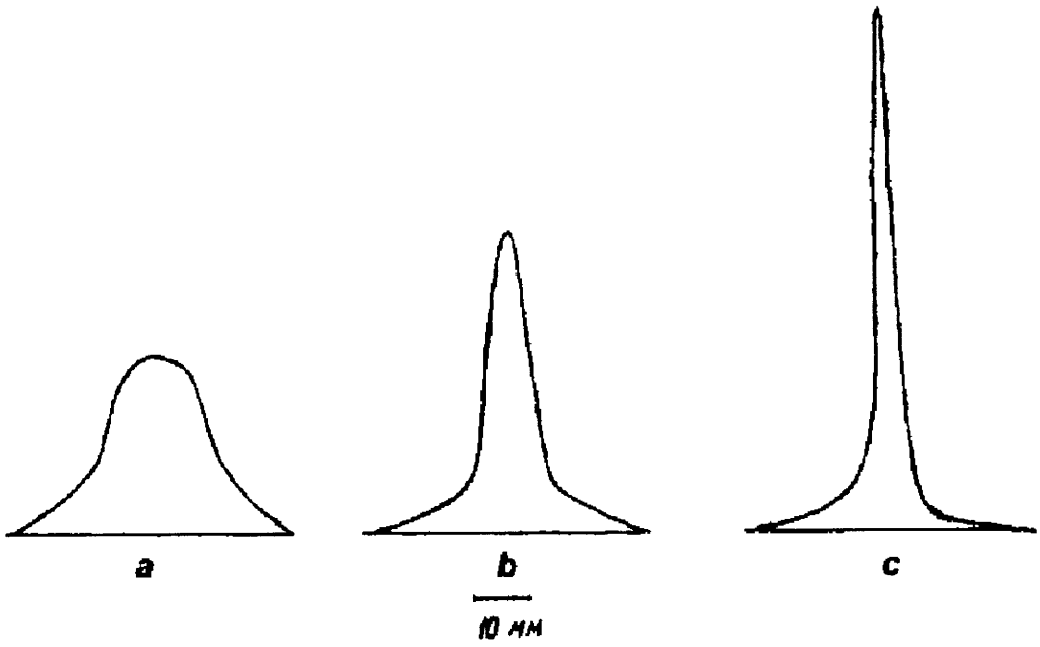

Figure 4-1: 5 MeV proton beam size (4.5 cm without focusing) after focusing with various plasma voltages (a. 4 kV, b. 7 kV, c. 9 kV) [31].

Chapter 5. Implementation of Plasma Arc

The creation of a stable plasma arc requires more than the application of high voltage between a cathode and an anode. The plasma arc will follow the path of least resistance which, in a gas, is the path of highest temperature. Due to this, the arc will move around as the thermal layers of the gas move. In order to stop this, the temperature variations in the gas must be well controlled throughout the process. These requirements are met by the "Plasma Porthole" created by Hershcovitch. The design and implementation of this device will be discussed in this chapter.

5.1 Plasma Porthole

The plasma porthole was designed to stabilize a plasma arc down the center of a small cylinder. This was accomplished by stacking thin copper plates (5 mm thick) with thin plates of boron-nitride (1.3 mm) in-between (Figure 5-1). Each of the plates had a small two mm hole drilled in the center and once all the plates were stacked, it formed a six cm long cylinder. Copper was chosen for its high heat conductance rate and overall heat characteristics. The plates were individually cooled by a chilled water supply and served to cool the gas on the outer edges of the cylinder. The outer cooling causes the warmest part of the gas to be at the center of the cylinder at all times. This stabilizes the thermal layers of the gas which in turn stabilizes the plasma arc.

A second criteria for creating a plasma arc is the isolation of the voltage potential through the gas. Since the current will seek out the least resistance possible, this isolation prevents the current from flowing through the structure instead of the gas. The boron-nitride plates between the copper cooling plates serve to isolate the plates from ground as

well as from each other. Care has been taken to prevent the plasma from coming in contact with the insulating plates to prevent them from melting. Each of the three structural bolts that hold the system together are covered by plastic sleeves and use plastic washers at the end to prevent them from creating a short. The three cathode holders are likewise isolated from the rest of the system by plastic sleeves.

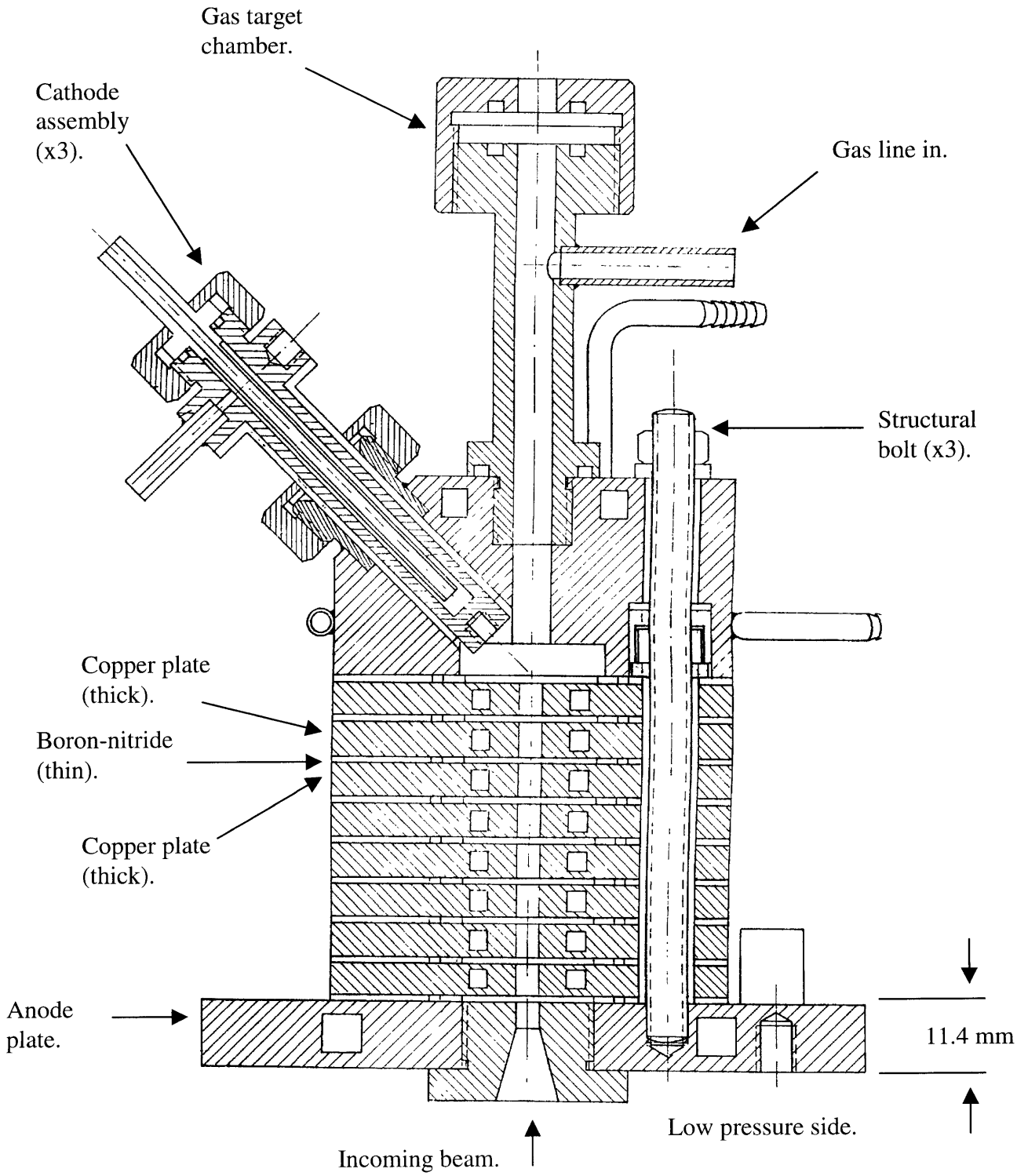

Figure 5-1: Cross section of plasma porthole [33].

5.2 System Installation

A new vacuum chamber system was assembled in order to test the plasma porthole. This system was created similar to the system previously discussed in order to allow for the use of the same vacuum pump arrangement. The previous vacuum chamber could not be used since its beam line was off center while the plasma porthole beam line is down the center. This new system was created by bolting three T-sections together to create the three pumping chambers. A solid aluminum plate was placed between each of the T-sections. Both plates had a thin tube (5 mm inner diameter, 96 mm long) attached to allow for constricted flow between each chamber. An end blanking plate was machined to mate to the plasma porthole and allow the device to be bolted to the last T-section (Figure 5-2).

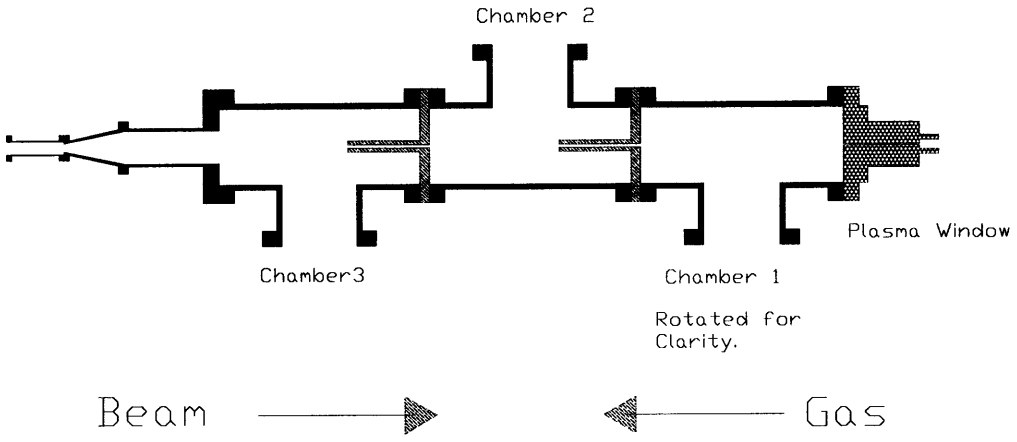

Figure 5-2: Plasma porthole system.

Once the plasma porthole was connected to the vacuum chambers, final connections were made. The target chamber was screwed into the front of the porthole and the necessary gas connections were made. A coarse and a fine valve were included in the gas line in a parallel arrangement. The fine valve was used to control the gas flow before the arc was created and then the coarse valve was used to raise the pressure afterward. Chilled water lines were connected to the system to provide cooling for the cathodes, copper plates, and anode plate. Finally, electrical lines were connected from the power supply to each of the cathode holders while the ground line was connected to the anode plate.

5.3 Expected Results

From discussions with Hershcovitch, we expected to achieve three atmospheres of pressure in the target chamber while maintaining 10^{-4} torr in the first vacuum chamber [25]. This pressure differential is dependent on the amount of energy that is inputted into the system. With higher energy, the temperature of the plasma gas is raised, thus raising the viscosity of the gas and decreasing the plasma flow. This can be clearly seen from previous experiments by Hershcovitch [26]. Since the electrons in hydrogen gas are more tightly bound than in argon, it is harder to create a plasma arc in hydrogen. This requires that a higher voltage be applied to achieve the same results.

VOLTAGE (V)	CURRENT (AMPS)	POWER (KW)	ΔPRESSURE (ATM)
193	50	9.7	3.1
208	50	10.4	3.8
158	50	7.9	1.3
196	40	7.9	3.4
203	50	10.2	3.5

Table 5-1: Pressure achieved at different power levels in argon [26].

Chapter 6. Applications

With the creation of a stable windowless target system, several of the previous limitations on accelerators can be removed. These limitations on beam current, energy focusing, and overall power output, have hampered many attempted accelerator applications. These applications will now benefit greatly from the new windowless target system.

6.1 Intense Fast Sources

With the removal of the limitations on the beam current and energy, it is now possible to create high intensity fast neutrons. The high energy of the neutrons greatly increases their range and allows for the imaging of larger objects. In a similar manner, the high beam current increases the radiation reaching the detector and reduces the time needed for recording data. This significant reduction in imaging time increases the throughput time of the system that has previously served as a limiting factor in many applications.

One program that will benefit greatly from both of these improvements is the nuclear stockpile stewardship. This project requires an imaging technique that can detect small defects in low-Z material that is surrounded by high-Z material in a nuclear device. The goal is to capture a full tomographic image within a few hours while being able to detect voids and other defects in the range of a cubic-mm. Previous experiments have proven the feasibility of this project with neutrons of energies between 4 and 400 MeV. These experiments drilled holes 4 to 12 mm in diameter in a 2.54 cm thick disk of LiD and placed it between two blocks of uranium (Figure 6-1). Preliminary experiments have

shown that similar results can be achieved with lower energy neutrons between 10 and 15 MeV and about $10^{12}/4\pi$ n/sec/sr [34,31].

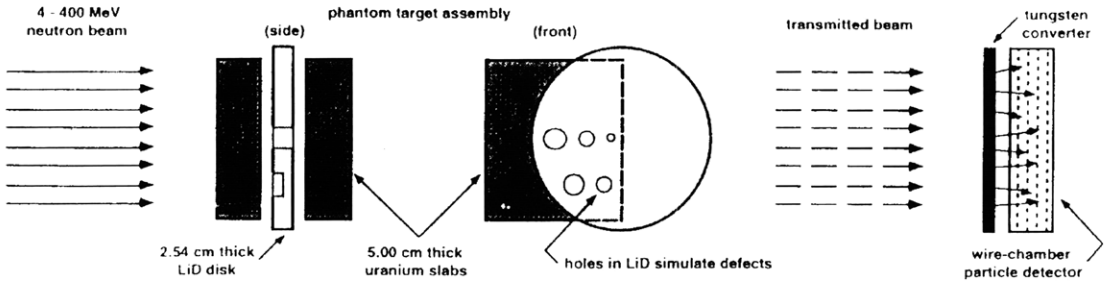

Figure 6-1: Proof of principal experiment for imaging low-Z material between blocks of high-Z material [35].

6.2 Monoenergetic Sources

Without a physical boundary to slow the accelerated particles down, the spread of neutron energies is greatly reduced. As shown previously, by choosing the reaction, characteristics of the accelerated beam, and the angle at which the neutrons are removed, it is possible to choose the neutron energy. This beam of tightly focused specific energy neutrons can be used to improve many imaging and detection techniques.

An important application that could take advantage of the energy focusing is the imaging of luggage for possible explosives. Studies have been conducted that pass neutron beams through luggage and analyze the transmitted spectrum. The neutron energies range from around 0.8 MeV at the lower end with an upper level between 4 and 8 MeV, depending on the experiment. Beams with such wide ranges of energies are

called "white" sources. The luggage is divided into pixels and the transmitted spectrum is analyzed for each pixel. The densities of H, C, N, and O are calculated with contributions from all other elements grouped into a fictitious element X. Since plastic explosives have high concentrations of N and O, the density information is used to establish a probability of the presence of plastic explosives. An improvement to this system can be gained by comparing this "white" neutron transmission spectrum to the transmission spectrum from a focused, monoenergetic neutron beam with energies between 4 and 5 MeV. As can be seen from Figure 6-2, the nitrogen cross-section is much higher for neutrons of this energy. By comparing these two transmitted spectrums, the difference will highlight the presence of nitrogen and greatly improve the accuracy of its density calculation [36, 37, 38, 39].

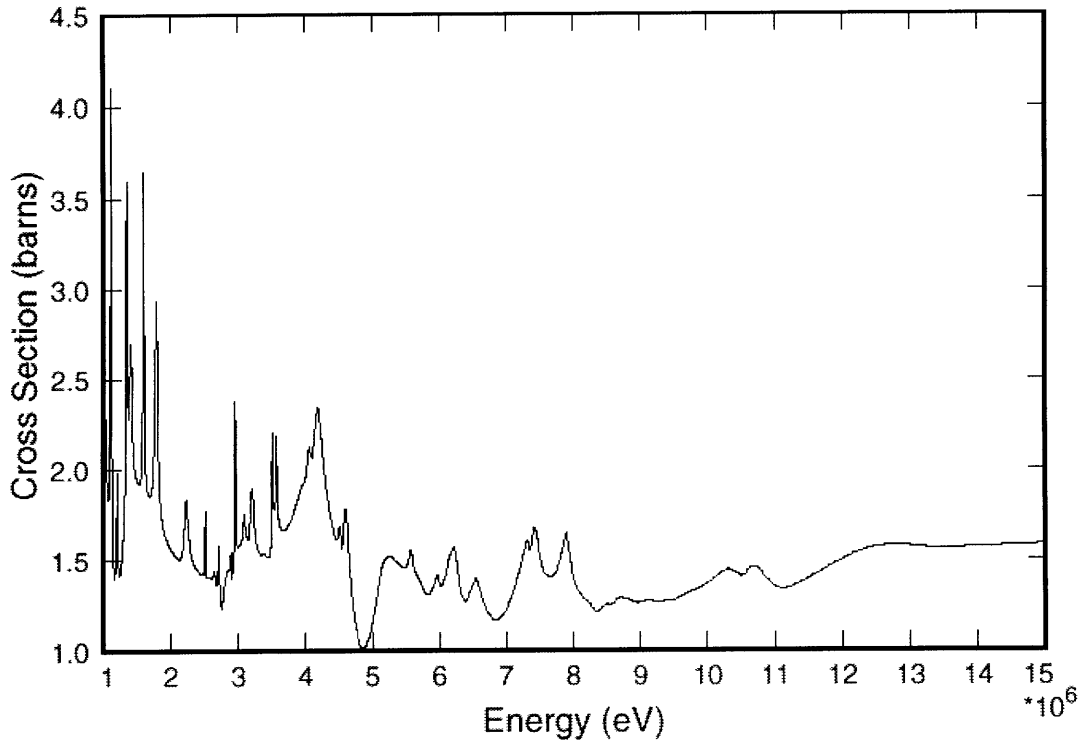

Figure 6-2: Total nitrogen cross-section versus neutron energy [40].

A second application that would gain from the comparison of "white" neutron transmission and monoenergetic neutron transmission is the search for dense carbon in unprocessed ore. In this system, small amounts of dense carbon are being removed from large amounts of ore and the system must be able to quickly distinguish and sort out the ore that contains the carbon. The total neutron cross-section for carbon contains a peak between 7 and 9 MeV (Figure 6-3) which can be used to identify it [18].

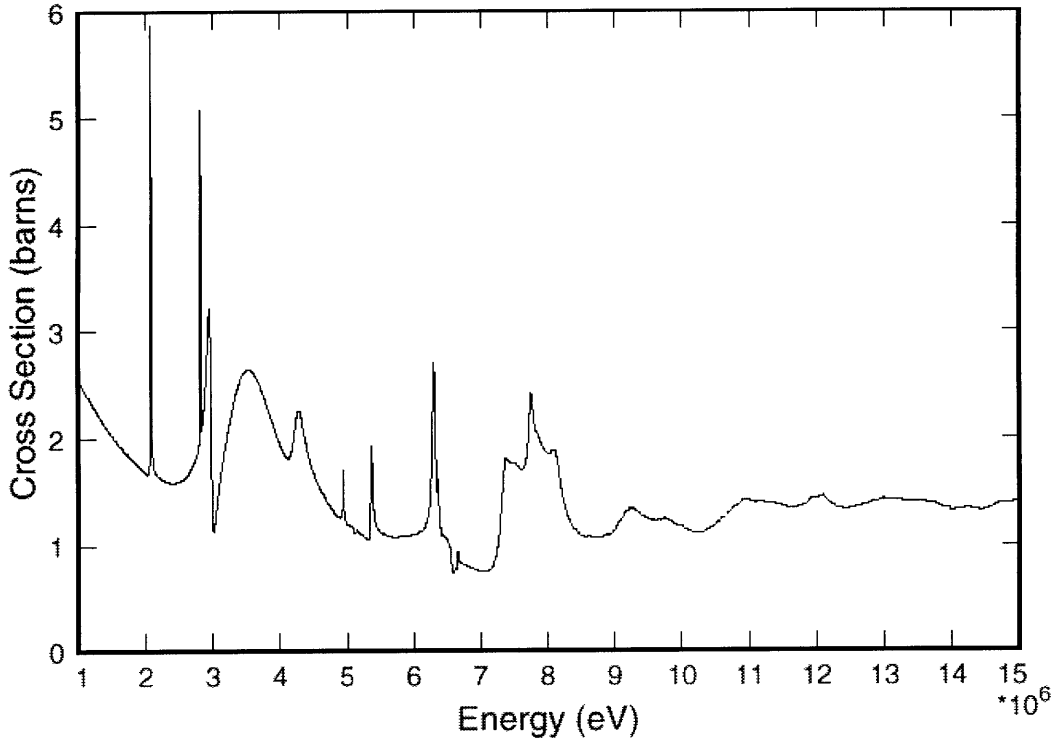

Figure 6-3: Total carbon cross-section versus neutron energy [40]

Both of these applications will also benefit from the reduction in scanning time that is gained from the increase in neutron flux as mentioned previously.

6.3. Accelerator-driven Transmutation of Waste (ATW)

Research has been conducted at Los Alamos National Laboratory to solve the problem of nuclear waste disposal by "burning" the long lived actinides in sub-critical assemblies. An accelerator is used to inject neutrons into the assembly which cause the long lived actinides to fission during sub-critical nuclear chain reactions. Multiple sub-critical assemblies are driven by a high energy proton accelerator that utilizes a 1000 MeV proton beam at 40 mA (40 MW) and a 100% duty cycle. The beam is split into different assemblies and in each it passes through a window and then into a liquid spalation target of lead or lead-bismuth eutectic. The liquid lead target also serves as a coolant for the sub-critical assembly and the window (Figure 6-4 and Figure 6-5). Removal of the physical window would allow for greater beam currents as well as a vastly improved life span for the target system [41, 42, 43].

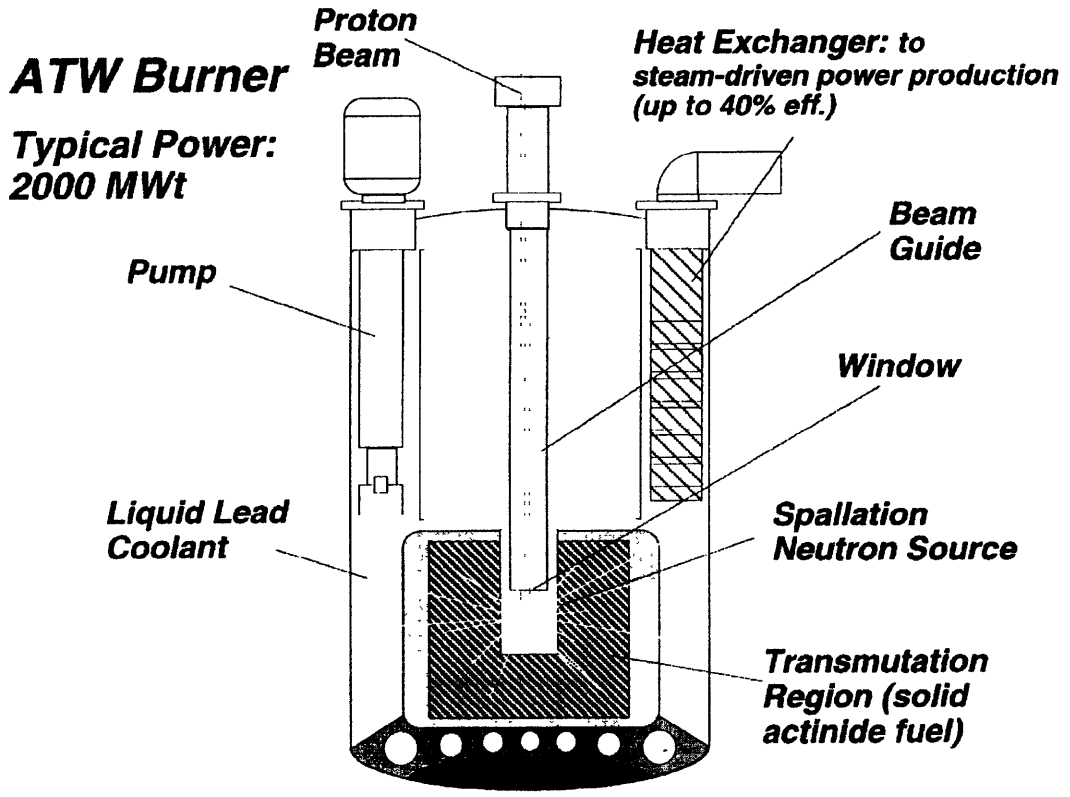

Figure 6-4: ATW target system [41].

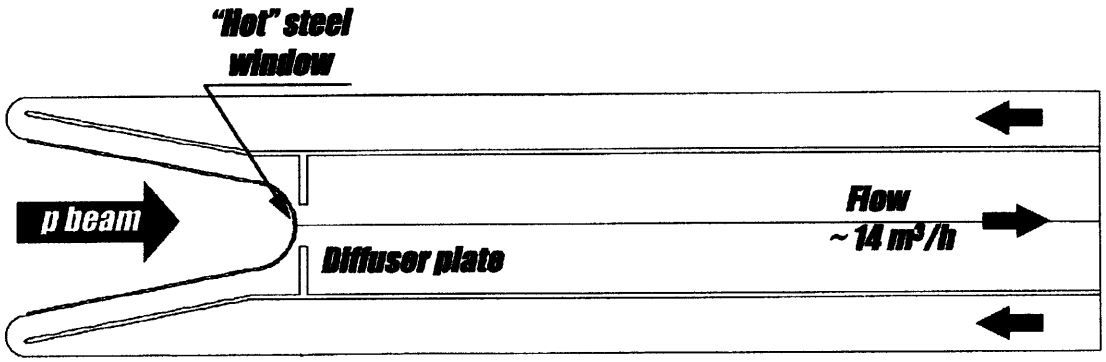

Figure 6-5: Enlarged view of window system with

cooling flow from liquid target [41].

Chapter 7. Conclusions and Future Work

Two separate windowless gas target systems have been investigated during this research. While the theory of both systems has been proven, neither one fully met the design goals of several atmospheres in the target chamber during previous experiments. Through the development achieved during this research, it is hoped that both systems will improve greatly in attainable pressures. It is at this point that we must ask whether one system is more advantageous than the other, and where should future efforts be invested.

7.1 Comparison

As shown in this report, the two systems differ vastly in their guiding principles. The mechanical system created by Iverson relies upon low conductance nozzles and rotating disks which open and close the beam pathway. The second system developed by Hershcovitch relies instead on the high pressure, low flow characteristics of a plasma arc along with low flow nozzles between chambers. This great difference in underlying principles results in vast differences in implementation.

The first and most obvious difference between the mechanical and plasma system is that the plasma system requires no moving parts. This removes a large degree of difficulty in design for the plasma window. The mechanical system will need to be precisely balanced to allow it to rotate at speeds that match the accelerators 640 Hz pulse rate. This also introduces difficulties in timing the accelerator pulse to the alignment of the holes. Finally, the added complication of high speeds components results in a greater likelihood that a part will break, possibly catastrophically. With the removal of moving components for the plasma system, all of these concerns are removed.

The addition of the plasma arc to the system adds different complications. First, the cooling requirements for the plasma channel must be met at all times during operation. Possible melting of the boron-nitride plates and the metal components could occur if there is an interruption in the chilled water supply. Cooling must also be provided for the first vacuum chamber to counteract the heat deposited from the small flow of plasma into the chamber. Without this cooling the chamber will be heated above acceptable limits within ten minutes [26]. The plasma window also requires a large power supply to strike and sustain the arc. Such a large power supply could be unwanted in some circumstances.

In the end, there are two final deciding factors that makes the performance of the plasma arc more desirable than the performance of the mechanical system. First, the plasma arc is designed to be operated steady state and allows for accelerator duty cycles of up to 100%. The mechanical system however relies upon the fact that the accelerator has a 2.25% duty cycle. Increases in the duty cycle would require that the holes in the disks be increased to allow for longer pulses which would reduce the efficiency of the disks and thereby reduce the efficiency of the overall system. The second deciding factor in favor of the plasma system is its favorable focusing effect on the deuteron beam. Such an effect is highly desirable in many applications and would reduce the need for other focusing devices.

While it is clear that the plasma arc system is more desirable than the mechanical system, it must be pointed out that the two systems are not mutually exclusive. It is possible to combine the two systems when higher target pressures are desired. Such a

system would combine the drawbacks of each system but may also allow for pressures which neither system could reach independently.

7.2 Future Work

This research has investigated and designed two separate windowless gas target systems for future experimentation. Some final assembly is required on each system before testing may begin but this should be easily accomplished. Once the systems are complete, tests should be run first with argon gas and without the accelerator beam running to allow for simple first approximation runs on each system. Once these are complete and the systems are well characterized, they should be aligned properly with the beam and the pressure tests should be recreated with deuterium gas. Depending on the results achieved from these initial runs, the beam should then be activated and the neutron flux should be measured. The maximum neutron flux will most likely be limited by radiation protection concerns rather then by any system constraints.

Appendix A. Pump Information

The following pages contain information on the WOD 900 B, TMU 520, TMU 260, and the UniDry 050. All of the information was taken from the Pfeiffer Vacuum Technology catalog [20].

Roots Vacuum Pumping Station WOD 900B.

Ordering number:	PPS42010
Type designation:	WOD 900 B
Price:	on request

The compact, serial pumping station for all applications in the rough and medium vacuum range.

Characteristics:

Flange (in)	DN 160 ISO-F
Flange (out)	DN 63 ISO-KF
Nominal pumping speed	900 m^3/h
Ultimate pressure: Total without gas ballast, smaller	$7.52 \cdot 10^{-05}$ Torr
Ultimate pressure: Total with gas ballast, smaller	$7.52 \cdot 10^{-05}$ Torr
Mains requirement: Voltage (selectable)	230/400 V, 50 Hz
Control cabinet	no
Version	With two stage backing pump

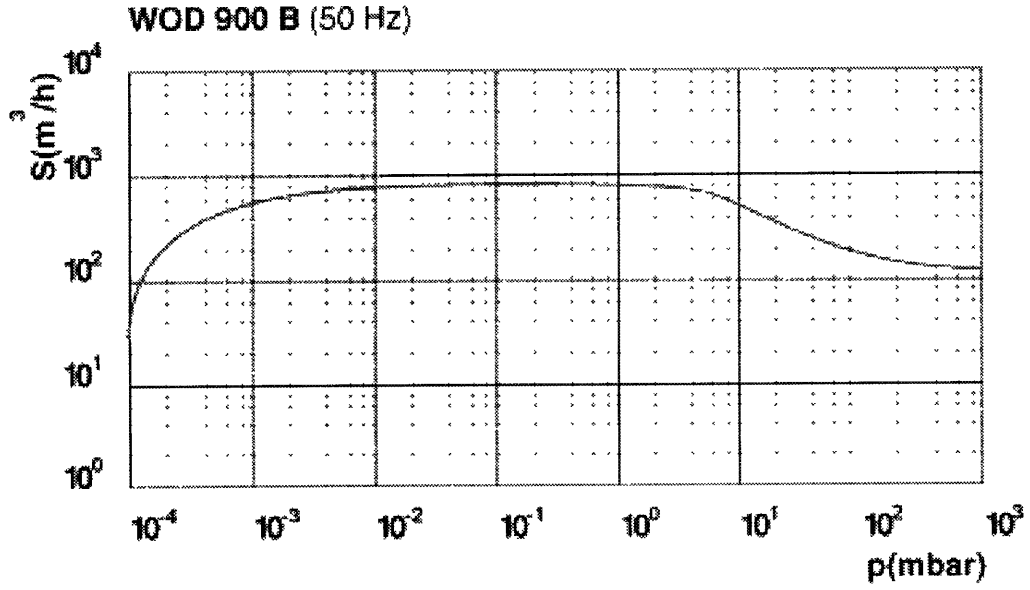

DN1 = DN 160 ISO-F
DN2 = DN 63 ISO-KF

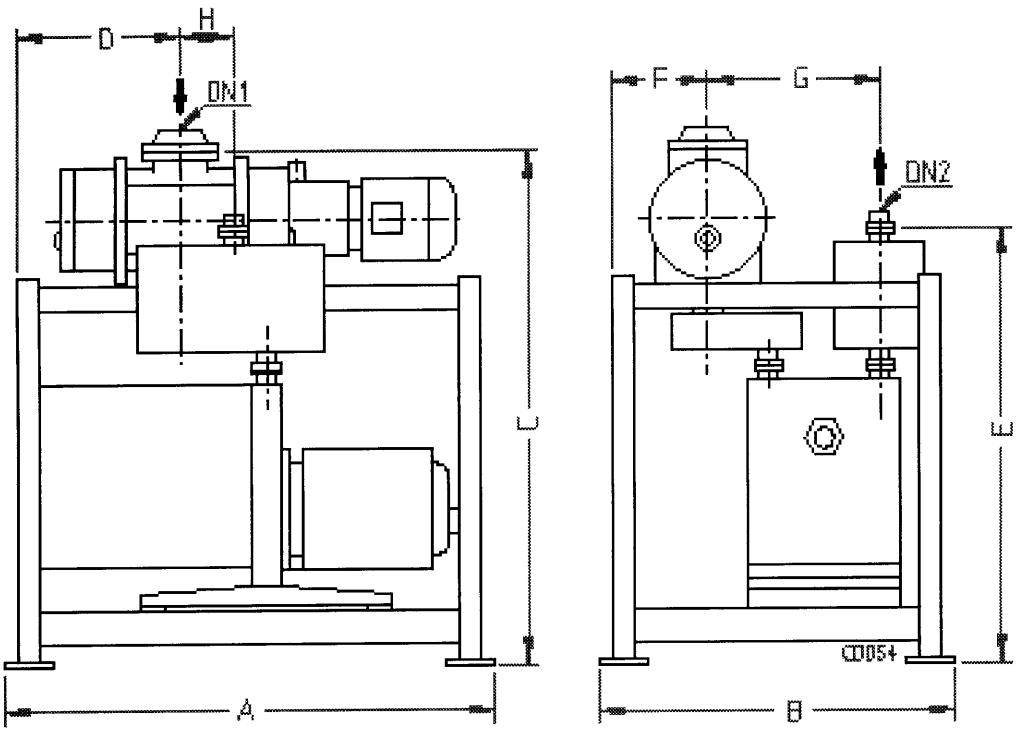

A = 1280 mm	B = 790 mm
C = 1330 mm	D = 430 mm
E = 1045 mm	F = 230 mm
G = 400 mm	H = 175 mm

Technical data:

Pumping station components	WKP 1000 A, ONF 063, DUO 120 A
Pumping speed	900 m^3/h
Switch on pressure	761.66 Torr
Ultimate pressure: Total without gas ballast, smaller	$3.76 \cdot 10^{-05}$ Torr
Ultimate pressure: Total with gas ballast, smaller	$3.76 \cdot 10^{-03}$ Torr
Water vapor tolerance	24.82 Torr
Pump fluid filling	4.23 gal (U.S.)
Pump fluid filling	4.23 gal (U.S.)
Motor rating total	7 kW
Motor rating total	7 kW
Mains requirement: Voltage (selectable)	230/400 V, 50 Hz, IP54
Mains requirement: Voltage (selectable)	230/400 V, 50 Hz, IP54
Weight	1168.43 lb
Weight	1168.43 lb

Turbomolecular Drag Pump TMU 520.

Ordering number:	PMP02430
Type designation:	TMU 520
Price:	13 200.00 US

The turbo drag pump with the edge in pumping speeds.

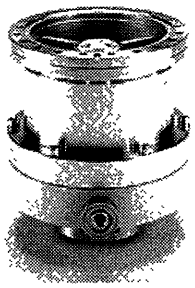

Industries

- Process Technology
- Lamps etc.
- Transportation
- Scientific

Characteristics:

Flange (in)	DN 160 CF-F
Flange (out)	DN 25 ISO-KF
Pumping speed: for N_2	500 l/s
Ultimate pressure with single stage rotary vane pump	$< 7.52 \cdot 10^{-11}$ Torr
Ultimate pressure with diaphragm pump	$< 7.52 \cdot 10^{-11}$ Torr
Gas throughput for N_2	236.69 sccm
Fore vacuum max. for N_2	12.03 Torr
Sealing gas connection	no

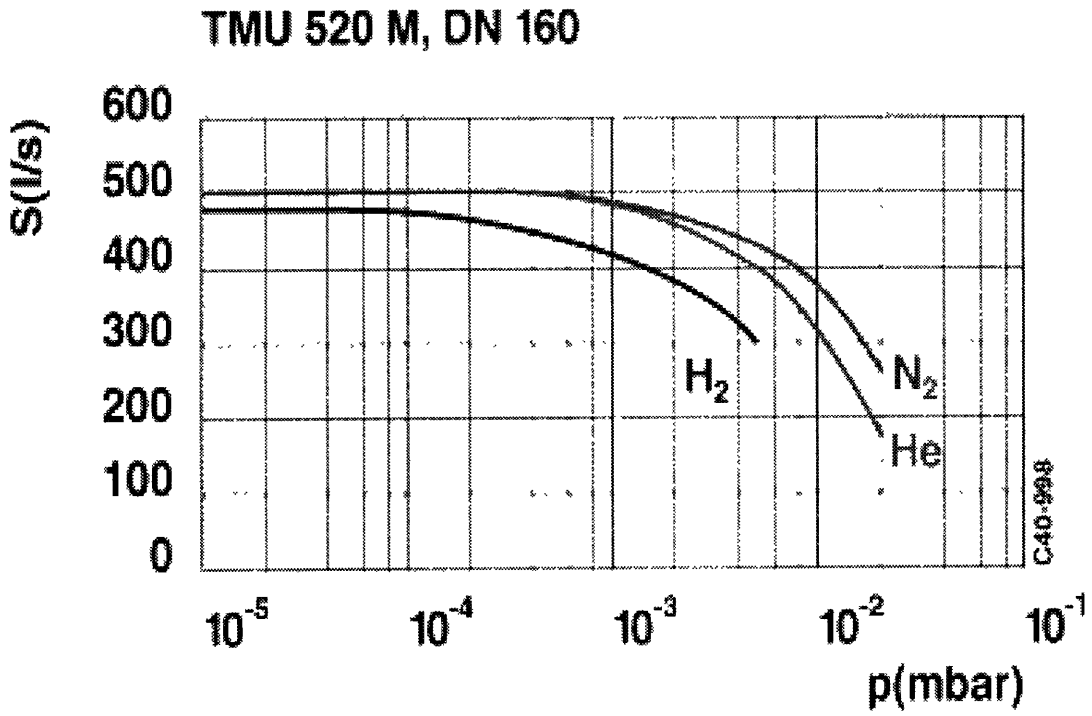

DN1 = DN 160 CF-F
DN2 = DN 25 ISO-KF

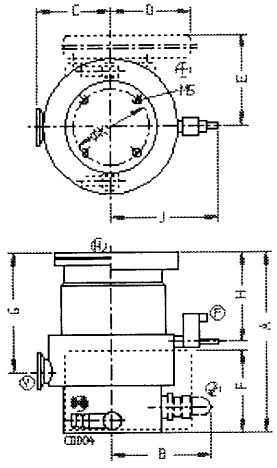

A = 224 mm	B = 115 mm
C = 122 mm	D = 64 mm
E = 170 mm	F = 127 mm
G = 166 mm	H = 119 mm
K = 86 mm	

Ⓗ High vacuum connection
Ⓕ Venting connection
⊕ Air cooling
Ⓥ Fore vacuum connection
Ⓩ Power connection
Water connection

Technical data:

Pumping speed: for N_2	500 l/s
Pumping speed: for He	500 l/s
Pumping speed: for H_2	480 l/s
Compression ratio for N_2	$1.00 \cdot 10^{12}$
Compression ratio for He	$5.00 \cdot 10^{07}$
Compression ratio for H_2	$5.00 \cdot 10^{06}$
Gas throughput for N_2	236.69 sccm
Gas throughput for He	414.21 sccm
Gas throughput for H_2	532.55 sccm
Ultimate pressure with single stage rotary vane pump	$< 7.52 \cdot 10^{-11}$ Torr
Ultimate pressure with diaphragm pump	$< 7.52 \cdot 10^{-10}$ Torr
Recommended roughing pump	MD 4T, DUO 010 M, UniDry
Rotational speed +-2%	50000 rpm
Rotational speed: Stand-by	33000 rpm
Run-up time with TCP 600	5 min
Cooling method, standard	water
Cooling water consumption	15 l/h
Weight	27.56 lb

Turbomolecular Drag Pump TMU 260.

Ordering number:	PMP02135
Type designation:	TMU 260
Price:	6 610.00 US

The turbo drag pump designed for a wide field of applications in industry and research.

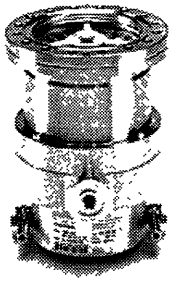

Industries
- Process Technology
- Lamps etc.
- Transportation
- Scientific
- Analytical

Characteristics:

Flange (in)	DN 100 CF-F
Flange (out)	DN 25 ISO-KF
Pumping speed: for N_2	210 l/s
Ultimate pressure with single stage rotary vane pump	$< 7.52 \cdot 10^{-11}$ Torr
Ultimate pressure with diaphragm pump	$< 7.52 \cdot 10^{-09}$ Torr
Gas throughput for N_2	147.93 sccm
Fore vacuum max. for N_2	7.52 Torr
Sealing gas connection	no

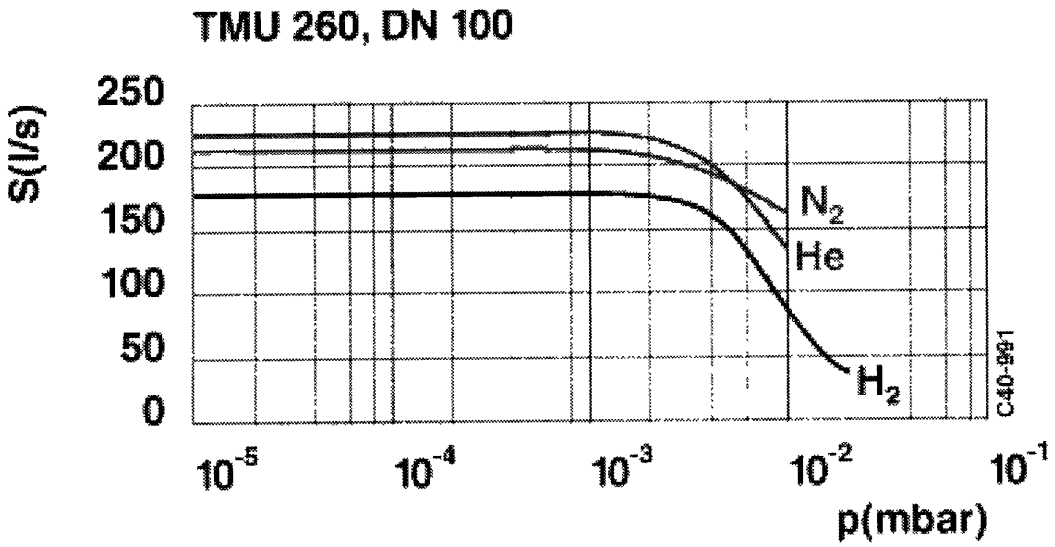

DN1 = DN 100 CF-F
DN2 = DN 25 ISO-KF

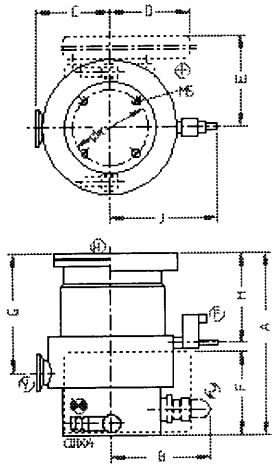

A = 194.5 mm
B = 115.0 mm
C = 82.0 mm
D = 64.0 mm
E = 135.0 mm
F = 127.0 mm
G = 128.5 mm
H = 95.0 mm
K = 86.0 mm

Ⓗ High vacuum connection
Ⓥ Fore vacuum connection
Ⓕ Venting connection
Ⓩ Power connection
⊕ Air cooling
Water connection

Technical data:

Pumping speed: for N_2	210 l/s
Pumping speed: for He	220 l/s
Pumping speed: for H_2	180 l/s
Compression ratio for N_2	$1.00 \cdot 10^{09}$
Compression ratio for He	$3.00 \cdot 10^{05}$
Compression ratio for H_2	13000
Gas throughput for N_2	147.93 sccm
Gas throughput for He	147.93 sccm
Gas throughput for H_2	118.35 sccm
Ultimate pressure with single stage rotary vane pump	$< 7.52 \cdot 10^{-11}$ Torr
Ultimate pressure with diaphragm pump	$< 7.52 \cdot 10^{-09}$ Torr
Recommended roughing pump	MZ 2T, UNO 005 A
Rotational speed +-2%	60000 rpm
Rotational speed: Stand-by	40000 rpm
Run-up time with TCP 380	1.5 min
Cooling method, standard	water
Cooling water consumption	15 l/h
Weight	19.85 lb

UniDry™ 050

Ordering number:	PKT11101
Type designation:	UniDry™ 050-4
Price:	on request

Standards:
– casing: nodular cast iron GGG 40.3
– casing seals: Viton
– radial shaft seals: PTFE
– operating fluid for gear box: F5 (filling not included)

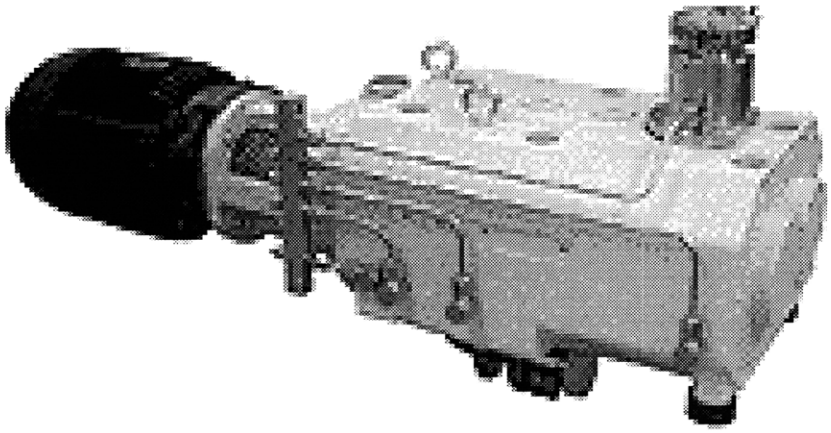

Characteristics:

Flange (out)	DN 25 ISO-KF
Version	with standard motor
Ultimate pressure, smaller	$3.76 \cdot 10^{-02}$ Torr
Mains requirement: Voltage (range)	230/400 V, 50 Hz
Pumping speed	50 m^3/h

Technical data:

Number of stages	4 pcs
Pumping speed at 50 Hz	50 m^3/h
Pumping speed at 60 Hz	60 m^3/h
Ultimate pressure	$< 3.76 \cdot 10^{-02}$ Torr
Intake pressure max.	751.88 Torr
Leak rate	5.92 sccm
Motor rating	3 kW
Power consumption	1.3 W
Rotational speed at 50 Hz	3000 rpm
Rotational speed at 60 Hz	3600 rpm
Cooling water consumption max.	3 l/h
Cooling water consumption at intake pressure	25 l/h
Cooling water temperature max.	25 °C
Cooling water pressure	2–10 bar
Cooling water connection, female thread	DIN ISO 228 G 1/2"
Cooling water connection	0.48 inch
Noise level with connected exhaust line	< 68 dB (A)
Lubricant amount in gear	$8.45 \cdot 10^{-02}$ gal (U.S.)
Ambient temperature	5–40 °C
Weight: without motor	253.53 lb
Weight: with motor	297.62 lb

Appendix B. Diagrams of Mechanical System

The following pages contain drawings of the re-designed mechanical system. All measurements are given in inches and no tolerances are shown. Section views are provided.

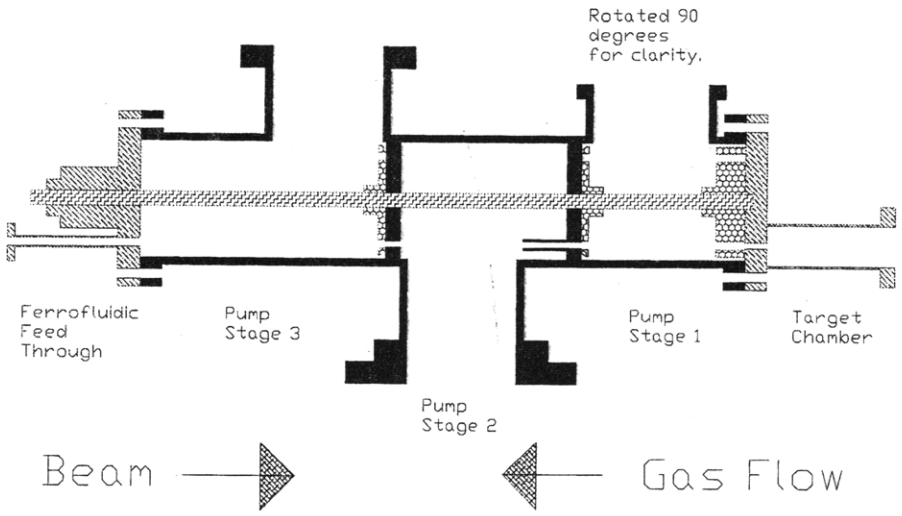

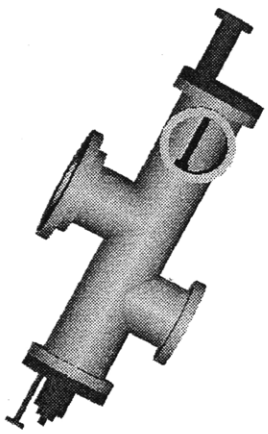

Vacuum Chamber

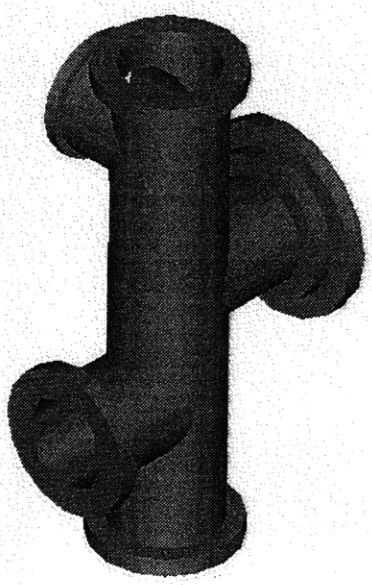

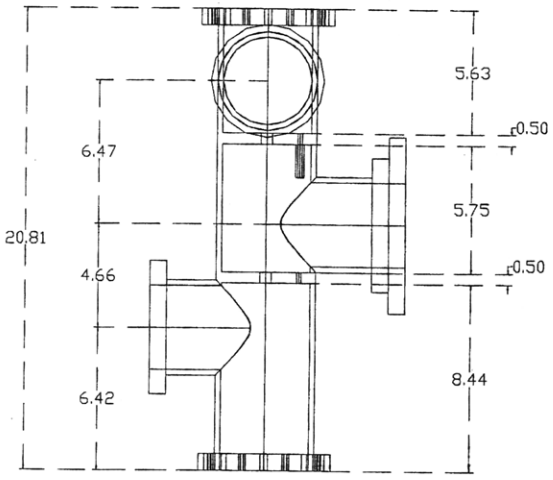

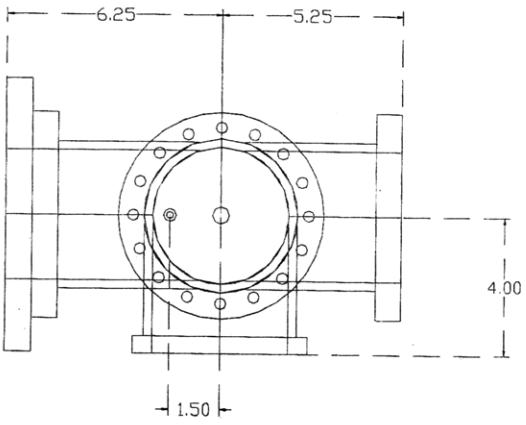

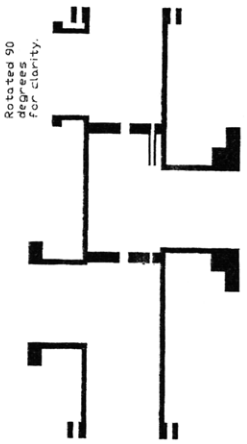

Disk 1

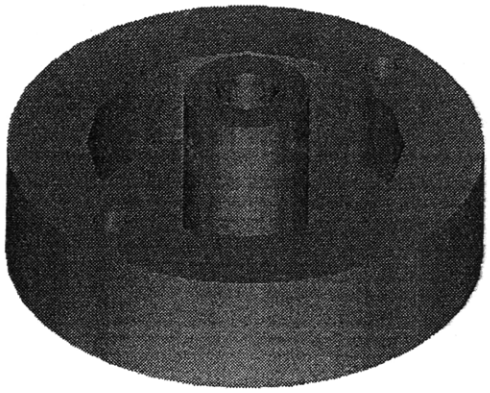

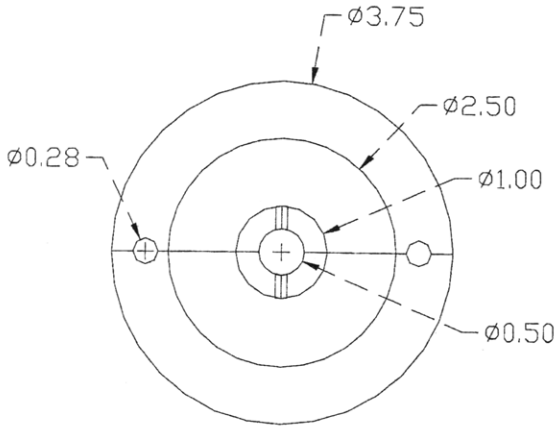

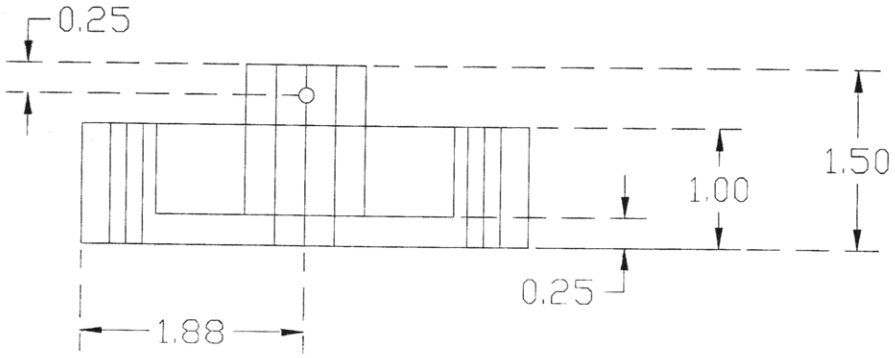

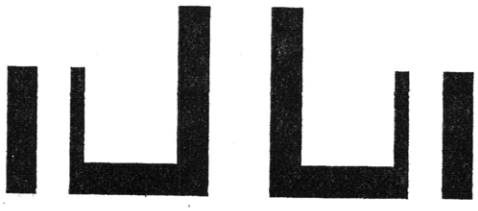

Disks 2 and 3

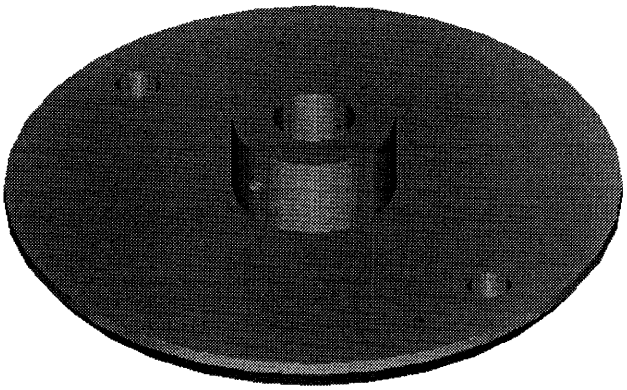

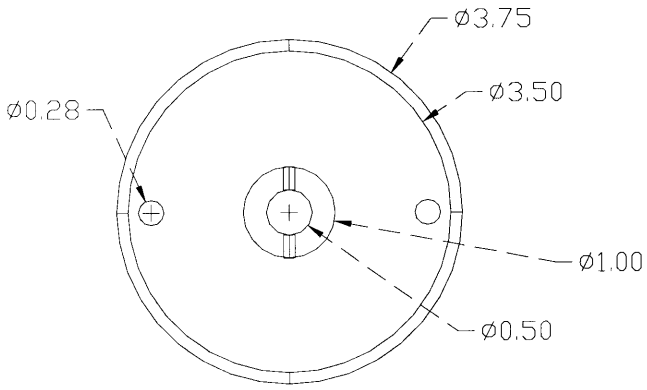

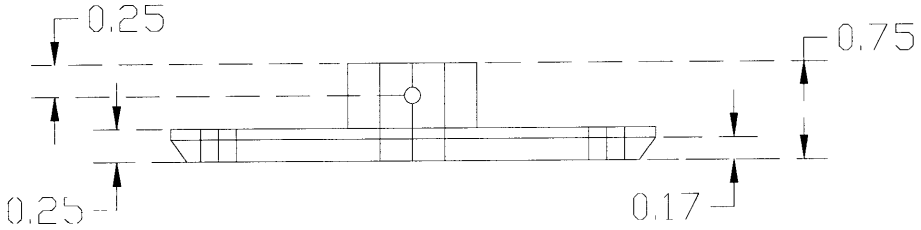

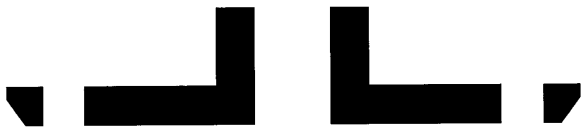

Rotary Feedthrough from Ferrofluidics

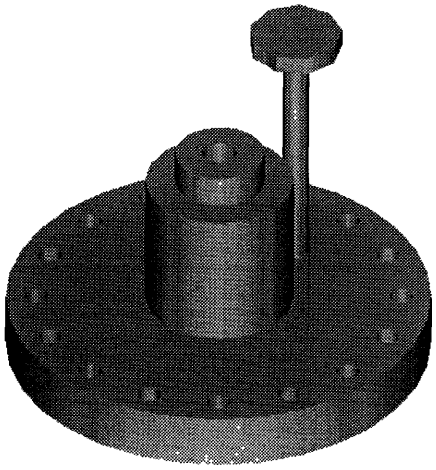

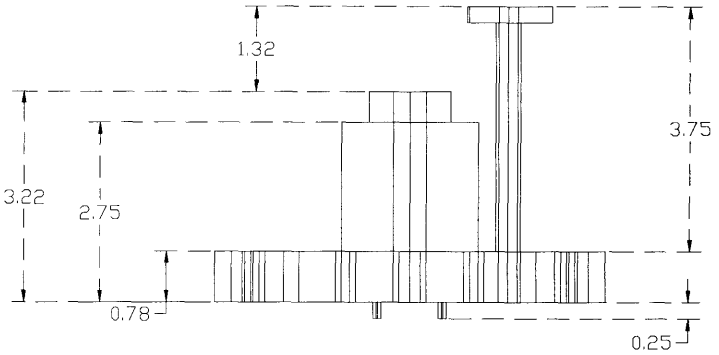

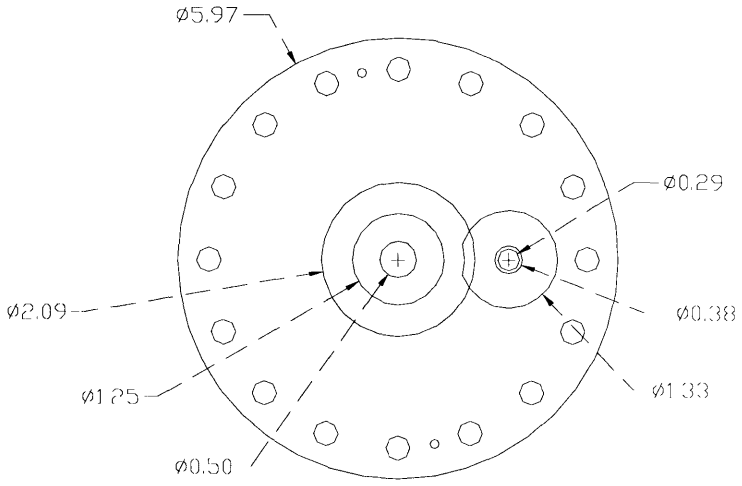

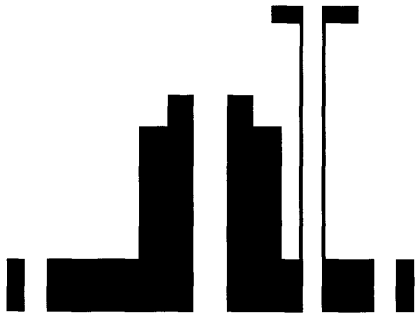

Target Chamber

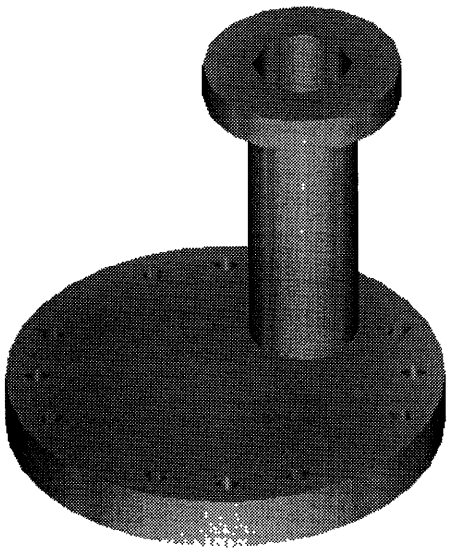

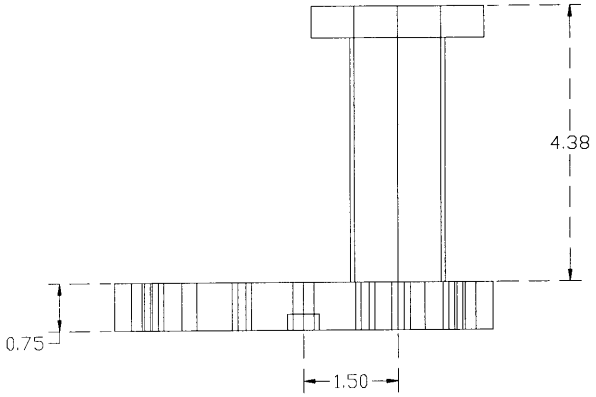

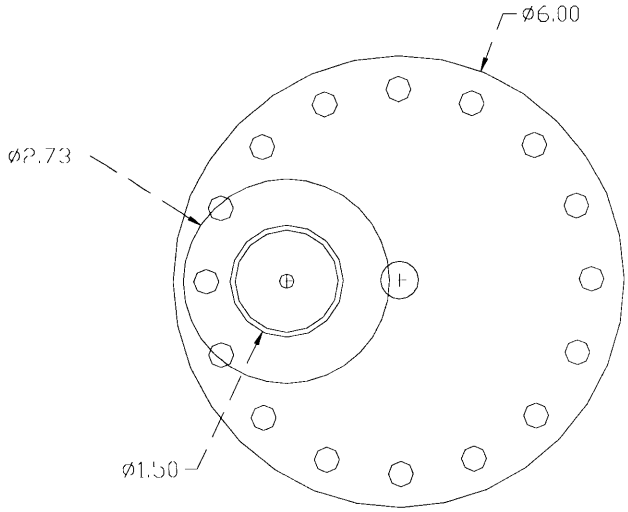

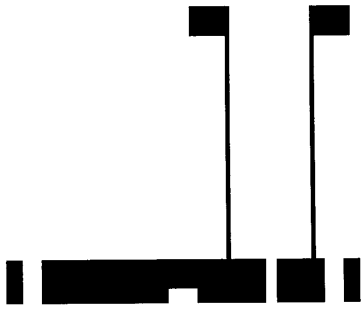

Appendix C. Diagram of Plasma Window System

The following pages contain drawings of the Plasma Porthole system. All measurements are given in inches except when stated, and no tolerances are shown. Section views are provided.

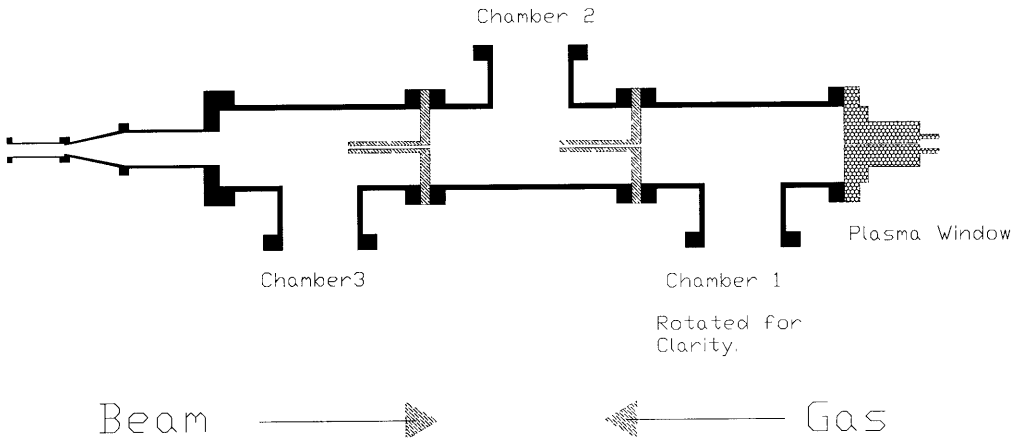

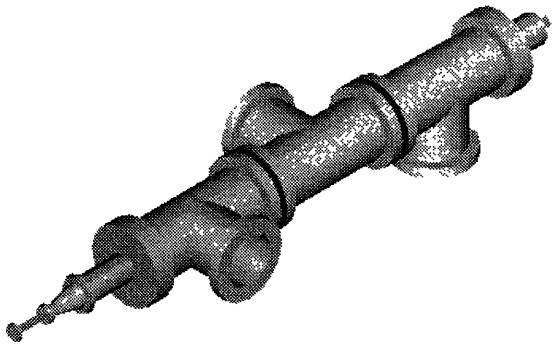

Vacuum Chamber

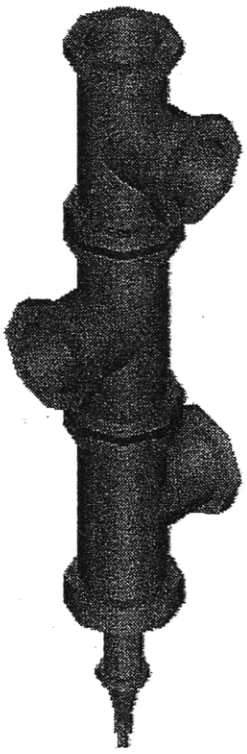

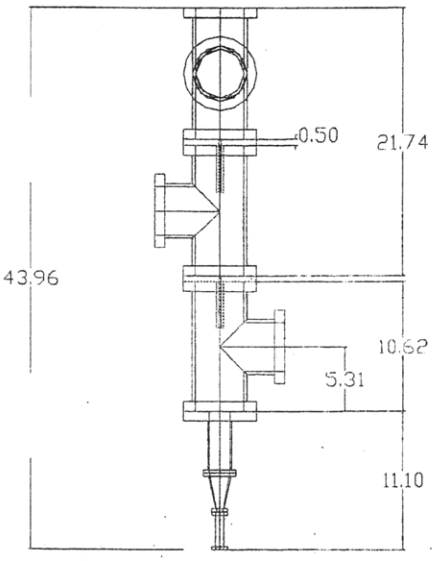

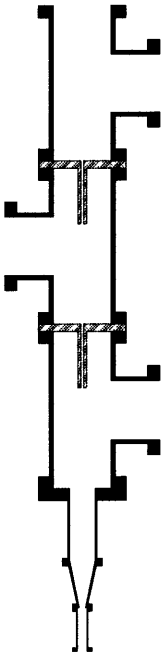

Rotated 90 Deg.
for clarity.

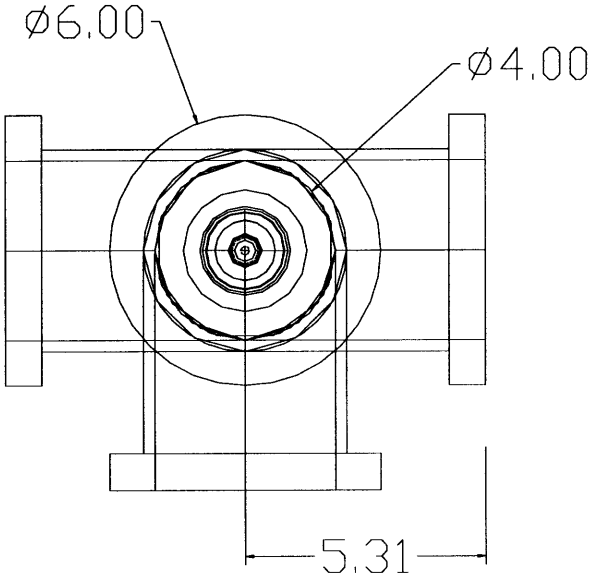

Plates and Low Flow Pipes

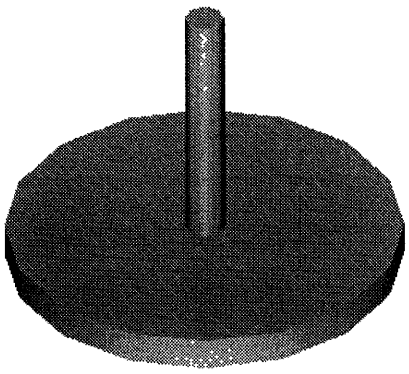

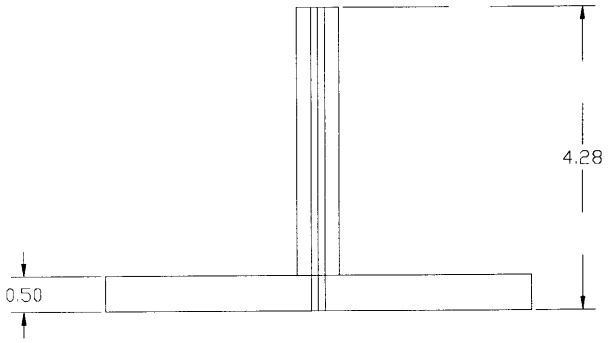

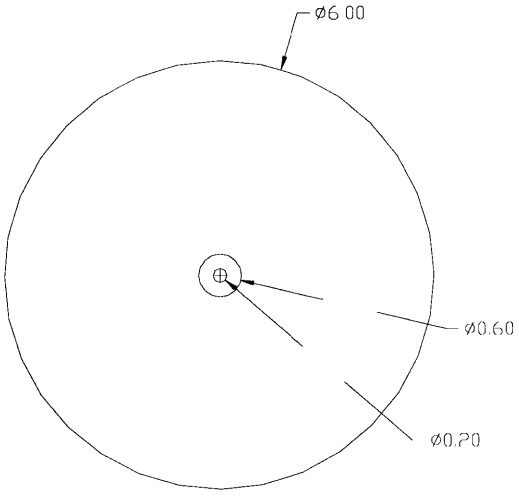

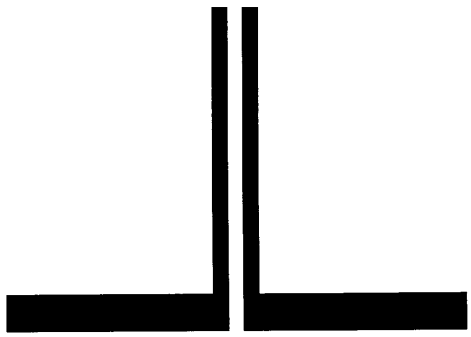

Plasma Window

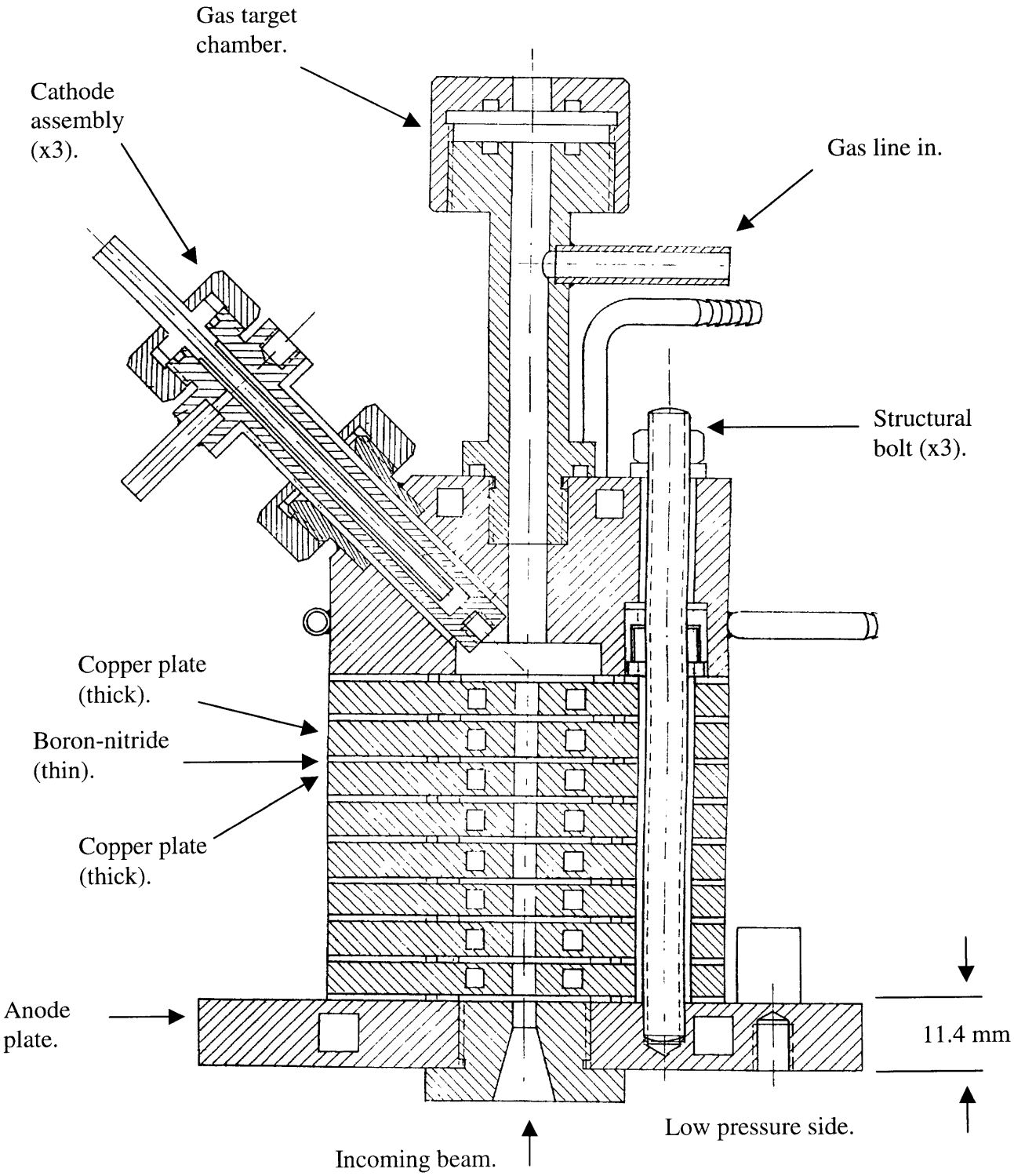

References

1. Turner, James E. *Atoms, Radiation, and Radiation Protection.* McGRAW-Hill, Inc. New York, 1992. Pp. 135-137.

2. Knoll, Glenn F. *Radiation Detection and Measurement.* Second Edition John Wiley and Sons, New York, 1989. Pp. 20-27.

3. Drosg, M. "Monoenergetic Neutrons in the Energy Range From 100 eV to 200 MeV From Two-Body Reactions With the Hydrogen Nuclei." *Neutrons in Research and Industry.* Vol. 2867, pp. 490-500, June 1996.

4. Iverson, Erik B. *Windowless Gas Targets for Neutron Production* Doctor of Philosophy Thesis. Massachusetts Institute of Technology. February 1997.

5. Carpenter and Yellon. *Meth. Exp. Phys.* Vol. 23, pp. 99-196, 1986.

6. Peto and Replenik. "High-Intensity 14-MeV Deuterium-Tritium Neutron Generators: Present Achievements and Future Potential." *Nuclear Science and Engineering.* Vol. 106, pp. 219-227, 1990.

7. Booth, Davis, Hanson et all. "Rotating Target Neutron Generations." *Nuclear Instruments and Methods.* Vol. 145, pp. 25-39, 1977.

8. Heikkinen, Logan, and Davis. "Rotating Target 14-MeV Neutron Generators." *Nuclear Science and Engineering.* Vol. 106, pp. 228-233, 1990.

9. Burke, Holmes, Johnson, Mann, and Miles. "SUPER-FMIT, an Accelerator Based Neturon Source for Fusion Components Irradiation Testing." *Nuclear Instruments and Methods in Physics Research B.* Vol. 10/11, pp. 483-486, 1985.

10. Carlson, David John. "Performance of a High-Pressure, High-Beam-Current Gas Target" *Nuclear Instruments and Methods.* Vol. 110, pp. 541-543 1973.

11. Mostafa. "Development and Performance of a High-Current Tritium Gas Target" *Nuvlear Instruments and Methods.* Vol 125, pp. 493-496, 1975.

12. Cramer and Cranberg. "Gas Target for Production of Monoenergetic Neutrons." *Nuclear Instruments and Methods.* Vol. 93, pp. 405-407, 1971.

13. Meadows, Smith and Winkler. "A High-Current Deuterium Gas Target For Neutron Nuclear Data Research." *Nuclear Instruments and Methods.* Vol. 176, pp. 439-442, 1980.

14. Haight and Garibaldi. "A Rotating Gas Cell for High-Intensity Monoenergetic Neutron Production." *Nuclear Science and Engineering.* Vol. 106, pp. 296-298, 1990.

15. Deleeuw, Haasz, Stangeby. "Canadian Gas Target Neutron Generator Research." *Nuclear Instruments and Methods.* Vol. 145, pp. 119-125, 1977.

16. Chenevert, Deluca, Kelsey, Torti. "A Tritium Gas Target as an Intense Source of 14 MeV Neutrons." *Nuclear Instruments and Methods.* Vol. 145, pp. 149-155, 1977.

17. Armstrong, Emigh, Meier, Meyer, and Schneider. "A 14 MeV Intense Neutron Source Facility." *Nuclear Instruments and Methods.* Vol. 145, pp. 127-148, 1977.

18. J.Watterson, Schonland Research Centre for Nuclear Sciences of the University of Witwatersrand, Johannesburg, private communications.

19. *Operation manual for Model DL-1 LINAC Neutron Generator System.* AccSys Technology, Inc. Pleasanton CA, October 1994.

20. *Vacuum Technology 1997* Catalog from Pfeiffer Vacuum. Nashua, NH 1997.

21. Rick Michaud and Jim Fraser at Ferrofluidics, private communications.

22. Mark Clement from Pfieffer Vacuum, private communications.

23. Hershcovitch, Ady. "High-pressure arcs as vacuum-atmosphere interface and plasma lens for nonvacuum electron beam welding machines, electron beam melting, and nonvacuum ion material modification." *Journal of Applied Physics.* Vol. 78 (9), November, 1995

24. Herscovith, Ady. "A Plasma Window for Transmission of Particle Beams and Radiation from Vacuum to Atmosphere for Various Applications." Accepted for publication.

25. Ady Hershcovitch from Brookhaven National Laboratory, private communications.

26. Data from Ady Hershcovitch, Brookhaven National Laboratory, private communications.

27. Fox and McDonald. *Introduction to Fluid Mechanics.* Fourth Edition. John Wiley & Sons, Inc. New York, 1992.

28. Gombosi, Tamas I. *Gaskinetic Theory.* Cambridge University Press, Great Britain, 1994.

29. Kim Molvig at MIT, private communications.

30. Leontovich, Acad., *Reviews of Plasma Physics, Volume 1.* Consultants Bureau, New York, 1969.

31. Belan et al. "Experiments on 5 MeV Proton Beam Focusing by Plasma Lens." *Review of Scientific Instruments.* Vol. 69, Number 2, pp. 1110-1112, February 1998.

32. Goncharov, Litovko, Onishchenko, Zadorozhny. "On 2D Electron Cloud Dynamics in High-Current Plasma Lens for Ion Beam Focusing." *Beam Stability and Nonlinear Dynamics.* The American Institute of Physics, 1997.

33. Cross section supplied by Peter Stefan from Brookhaven National Laboratory.

34. Hall, Dietrich, Logan. "Development of High-Energy Neutron Radiography." Unpublished.

35. Dietrich, Hall, Logan. "Conceptual Design for a Neutron Imaging System for Thick Target Analysis Operating in the 10-15 MeV Energy Range." *Application of Accelerators in Research and Industry.* AIP Press, New York, 1997.

36. Overley et al. "Results of Tests for Explosives in Luggage From Fast-Neutron Time-of-Flight Transmission Measurements." *Neutrons in Research and Industry.* Vol. 2867, pp. 219-222, June 1996.

37. Miller, Staagen, Gibson, Krauss. "Contraband Identification in Sealed Conatiners Using Neutron Transmission." *Neutrons in Research and Industry.* Vol. 2867, pp. 215-218, June 1996.

38.. Lefevre et al. "Using a Fast-Neutron Spectrometer System to Candle Luggage for Hidden Explosives." *Neutrons in Research and Industry.* Vol. 2867, pp. 206-210, June 1996.

39. Chmelik et al. "Analysis of Blind Tests for Explosives in Luggage Through Fast-Neutron Transmission Spectroscopy." Unpublished. January 1997.

40. "Nuclear Data Viewer." Las Alamos National Laboratory. Viewed April 28, 1998. http://t2.lanl.gov/data/ndviewer.html.

41. Browne, Venneri, Li, Williamson. "Accelerator-Driven Transmutation of Waste." Los Alamos National Laboratory, un-published.

42. MIT ATW Technical Review, January 15-16, 1998.

43. M. Kazimi from MIT, private discussion.